Integrated Master's in Chemical Engineering

Synthesis and characterization of doped 2D materials

A Master's Dissertation

by

Hélder Filipe Verdade da Silva Fontes

Developed within the course of Dissertation

held in

Associate Laboratory LSRE-LCM

Supervisors:
Professor Joaquim Luís Bernardes Martins de Faria
Doctor Eliana Sousa da Silva

Departamento de Engenharia Química

June of 2019

Acknowledgments

This page is dedicated to all people who deserve a special thanks and that helped me throughout my life. I can't specify all of them, otherwise I would need to right another dissertation just to thanks everyone in detail. However, the following deserve a special acknowledgement:

To the financing entities, in which this work was financially supported: Project POCI-01-0145-FEDER-029600 (2DMAT4FUEL), funded by European Regional Development funded by FEDER funds, through COMPETE2020 – Programa Operacional Competitividade e Internacionalização (POCI) and by national funds (PIDDAC) through FCT/MCTES. Projects: NORTE-01-0145-FEDER-000006 - funded by NORTE2020 through PT2020 and ERDF; Associate Laboratory LSRE-LCM - UID/EQU/50020/2019 - funded by national funds through FCT/MCTES (PIDDAC).

To my two supervisors, Professor Joaquim L. Faria and Doctor Eliana da Silva. Without both of you I wouldn't be able to do and deliver this dissertation. All of your teachings, suggestions and availability will, without a doubt, leave a mark in my life.

To the director of the LCM, Professor José Figueredo for giving the access to all the laboratory infrastructure. To Professor Pedro Tavares (UME, UTAD) for performing the XRD analysis and to the team of CEMUP (Porto) for performing the SEM analysis.

To all lab co-workers and colleagues, with a special note to Hanane Boumeriame, who was here all the time, not thinking twice in helping me. Also, our chats certainly helped me see things in another perspective.

To my family, in particularly to my parents, who were always there during these 23 years of life, not just during this dissertation. During my sad and happy moments, you were, without a doubt, the cornerstone of my life. A simple acknowledgment is not enough, so, I hope I can make you proud throughout the rest of my life.

To my girlfriend, Xana, thank you for all the attention and help. When I was in need you were always there to help me lift up and with a smile you made everything better. I like to think I had the same effect in you. I hope we can continue creating new memory of those good moments.

To all of my friends, that I knew throughout my life, thank you for all of your availability and happy moments. I will always cherish those moments in my heart. I can't specify all of you, however your support was also an important pillar in this dissertation.

Abstract

The development of new, inexpensive, and easy-prepared materials is a key factor in the XXI century. In particular, the development of selective catalysts that can produce fuels is an important landmark in energy production.

Different 2D photocatalysts based on graphitic carbon nitride (g-C_3N_4) and reduced graphene oxide were prepared by the thermal decomposition of dicyandiamide and the Hummers method, respectively. Several modifications to bulk g-C_3N_4 were also applied to suppress some of its limitations, including a thermal treatment to exfoliate its sheets, as well as metal deposition and non-metal doping and creation of composites. The first approach was the doping of g-C_3N_4 with metal elements (Au, Pd, Pt and Ru). Nevertheless, metal co-catalysts are expensive and their resources are scarce. Therefore, another co-catalyst was studied, molybdenum disulfide (MoS_2), to produce a greener route towards the production of selective photocatalysts for solar fuels. In particular, for the composite with g-C_3N_4, two synthesis methods were studied, the impregnation and the *in-situ*. It was proven that the synthesis route has a great influence in the resulting material. This co-catalyst was also tested in reduced graphene oxide. The second approach consisted in doping g-C_3N_4 with non-metal elements (phosphorus and phosphorus-oxygen), followed by preparing composites with MoS_2. All of the materials were characterized by photoluminescence, UV-Vis diffuse-reflectance and infra-red spectroscopies, N_2 adsorption-desorption and scanning electron microscopy analysis. Transmission electronic microscopy was also performed for the g-C_3N_4 doped with metals while X-ray diffraction was only used to study the crystal structures of g-C_3N_4 with MoS_2. The materials were also screened for the photocatalytic production of H_2 by visible-light irradiation using Light Emitting Diodes (LEDs).

Doping g-C_3N_4 with metals resulted in a significant increase in the production of H_2. In particular, when Ru was loaded in the g-C_3N_4 exfoliated material, a production of 16.904 $mmol \cdot g^{-1} \cdot h^{-1}$ of H_2 was obtained, far superior than the reported literature. MoS_2 was proven to be an effective co-catalyst, with the synthesis method playing a significant role in the composite activity. The *in-situ* method allowed the forming of a more efficient heterojunction between the two phases, as corroborated by the characterization techniques, resulting in a superior photocatalytic performance. The doping of phosphorus caused changes in the physical-chemical properties of bulk g-C_3N_4, thus increasing the photocatalytic H_2 production.

Keywords: 2D materials; photocatalysts; graphitic carbon nitride; graphene oxide; molybdenum; disulfide; photocatalytic hydrogen production

Resumo

O desenvolvimento de novos materiais que possuam um custo reduzido e que sejam simples de preparar é um fator essencial para o desenvolvimento da nossa sociedade. Principalmente, o desenvolvimento de catalisadores seletivos para a produção de combustíveis, é um ponto crucial na produção da energia e no modo como a energia é vista.

Diversos foto-catalisadores 2D baseados em nitreto de carbono grafítico (g-C_3N_4) e óxido de grafeno reduzido foram preparados por decomposição térmica da dicianodiamida e pelo método de Hummers modificado, respetivamente. O g-C_3N_4 de base foi modificado de modo a suprimir algumas de suas limitações, nomeadamente, através de um tratamento térmico para esfoliar a estrutura em camada, de deposição/dopagem com metais e não-metais, ou preparação de compósitos.

A primeira abordagem na síntese destes materiais foi a introdução de metais (Au, Pd, Pt and Ru). No entanto, estes metais são dispendiosos e as suas reservas limitadas. Com isto em mente, abordou-se o dissulfureto de molibdénio (MoS_2), com vista a tornar a síntese de catalisadores seletivos para a produção de combustíveis solares mais verde. Em particular, para o compósito com g-C_3N_4 foram testados dois métodos: impregnação e síntese "*in-situ*". Ficou estabelecida a importância do método de síntese nas características catalíticas do material resultante. O MoS_2 foi também combinado com óxido de grafeno reduzido. A segunda abordagem consistiu em dopar o g-C_3N_4 com elementos não metálicos (fósforo e oxigénio), seguindo-se a preparação de compósitos com MoS_2. Todos os materiais foram caracterizados por espectroscopias de fotoluminescência, refletância difusa UV-Vis e de infravermelho, isotérmicas de adsorção-dessorção de N_2, e microscopia eletrónica de varrimento. Para os materiais de g-C_3N_4 modificados com metais usou-se também microscopia eletrónica de transmissão e para os materiais de g-C_3N_4 com MoS_2 a difração de raios-X. Estes materiais foram testados para a produção fotocatalítica de hidrogénio por irradiação de luz visível usando Díodos Emissores de Luz (*Light Emitting Diodes*, LEDs).

A dopagem de g-C_3N_4 com metais foi especialmente eficiente no processo de produção fotocatalítica de hidrogénio. Em particular, para o Ru sobre o g-C_3N_4 esfoliado, a produção de H_2 (16.904 $mmol \cdot g^{-1} \cdot h^{-1}$) foi muito superior à reportada na literatura. Foi também demonstrada a importância do MoS_2 como co-catalisador, sobretudo quando se usou o método de síntese *in-situ* que conduziu à formação de uma heterojunção eficiente entre as duas fases. Tal foi corroborado pelas técnicas de caracterização usadas e pelos resultados de atividade fotocatalítica. Também a dopagem com fósforo conduziu a um aumento da produção fotocatalítica de H_2.

Palavras-chave: materiais 2D; fotocatalisadores; nitreto de carbono grafítico; óxido de grafeno; dissulfureto de molibdénio; produção fotocatalítica de hidrogénio

Declaration

I hereby declare, on my word of honor, that this work is original and that all non-original contributions were properly referenced with source identification.

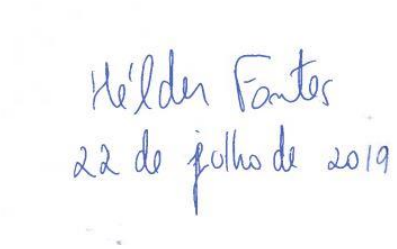

Sign and date

Index

List of Figures

List of Tables

Notation and Glossary

List of Acronyms

EtOH	Ethanol
EDTA	Ethylenediaminetetraacetic acid
FTIR	Fourier transformed infrared spectroscopy
GC	Gas chromatography
GO	Graphene oxide
GCN	Bulk graphitic carbon nitride
GCN(T)	Exfoliated graphitic carbon nitride
GCNM	Bulk graphitic carbon nitride doped with metals
GCN(T)M	Exfoliated graphitic carbon nitride doped with metals
GCNMxxI	Composites of bulk graphitic carbon nitride and MoS_2 (xx represents the wt%) prepared by impregnation
GCNMxxA	Composites of bulk graphitic carbon nitride and MoS_2 (xx represents the wt%) prepared *in-situ*
GCNP	Bulk graphitic carbon nitride doped with phosphorus
GCNPO	Bulk graphitic carbon nitride doped with phosphorus and oxygen
GCNPMxxA	Composites of phosphorus doped bulk graphitic carbon nitride and MoS_2 (xx represents the wt%) prepared *in-situ*
GCNPOMxxA	Composites of phosphorus and oxygen doped bulk graphitic carbon nitride and MoS_2 (xx represents the wt%) prepared *in-situ*
LDH	Layered double hydroxide
LEDs	Light emitting diodes
MeOH	Methanol
PL	Photoluminescence spectroscopy
rGO	Reduced graphene oxide
SEM	Scanning electron microscopy
TEM	Transmission electron microscopy
UV-Vis	Ultraviolet-visible diffuse reflectance
XRD	X-ray diffraction

1 Introduction

Modern society has a massive impact on our planet, especially developed countries, who are accustomed to a particular lifestyle. This has a significant contribution to the scarcity of natural resources on our planet. In particular, the enormous consumption of fossil fuels, to cope with our lifestyle, has not only an impact in the depletion of resources but also has a major role in climate changes, mainly due to the massive release of carbon dioxide, CO_2, the most prevalent greenhouse gas. This climate changes not only reflect on the increasing worldwide temperature, but also in air and water quality[1].

Human activity causes about 37 Gt of CO_2 emissions every year, and about 80% of these emissions are due to energy or energy-related activities[2]. Many researchers estimate that the concentration of CO_2 increased by about 31% over the past 200 years (since the beginning of the industrial revolution)[3].

However, changes in this paradigm are not as easy as one can think. The foundations of our global economy are highly dependent on oil and coal, the most widely used fossil fuels. So, when addressing the energy crisis, we need to have in mind that there is also an economic and political crisis associated which can be seen, over the past few years, by an aggressive and not-healthy competition for fuels, leading to war and unjust social problems.

Since these problems became more global, politics and researchers focused their attention on developing new sources or new forms of exploiting energy, such as renewable types. However, these renewable sources of energy are usually associated with expensive equipment and low efficiency. Therefore, if we could use solar light as a source to produce fuels, an energy crisis could be avoided.

A solar fuel that has grasped the attention of the scientific community is hydrogen (H_2). Its production by heterogeneous photocatalysis is a promising route towards sustainability. However, one of the critical drawbacks of production of H_2 through water splitting is the semiconductor/photocatalyst materials used not being selective towards its generation or not producing the desirable amounts.

Another way towards the sustainability of energy is to use CO_2 to produce fuels. This is a two-in-one approach. By one hand we would produce fuels, that can be used instead of non-renewable sources, and decreased the amount of CO_2 in our atmosphere, reducing the greenhouse effect[4]. This is the main target of the photocatalytic reduction of CO_2, using solar irradiation as a light source. Some studies have already been done in this subject, being one of the most promising routes towards sustainability in energy.

Since the early stages of the photocatalytic reduction of CO_2 and H_2 production, many materials have been tested, with several different conditions, such as metal sulfides, metal oxides, carbon materials and metal-organic frameworks[4-6]. However, these materials are usually inefficient and not selective. Low absorption of visible light and high recombination of electron-hole are some of the major issues associated with these materials. Therefore, the need to develop new materials that can be selective and efficient, while not being expensive and, preferably, without noble metals, is of extreme importance.

In the past few years, several new two-dimensional (2D) carbon materials, such as graphitic carbon nitride and graphene, have been studied and applied in different reaction conditions[6,7]. These new materials possess many exciting qualities, such as a high specific surface area and chemical and physical stability. Also, having a thickness of few atoms improves the light absorption and exploitation[4].

The primary goal and contribution of this Dissertation, is the development of new photocatalysts, mainly 2D materials, that can be applied to solar fuels production. Materials based on graphitic carbon nitride, molybdenum disulfide and reduced graphene oxide were synthesized. Their characterization by UV-Vis diffuse reflectance, infra-red and photoluminescence spectroscopies, scanning and transmission electron microscopies, X-ray diffraction and isotherm analysis, was performed. Finally, the activity of the materials was tested towards the photocatalytic production of hydrogen through water splitting using Light Emitting Diodes (LEDs) as a visible light source.

1.1 Contributions of the Work

All the synthesis procedures, characterizations and solar fuels production were performed by me except where indicated, as in the synthesis of the reduced graphene oxide/MoS_2 composites, which were produced by Doctor Luísa Maria Pastrana-Martinez, a researcher at University of Granada (Spain).

1.2 Organization of the thesis

This thesis is organized into five chapters to create a logical view of the subject. Whitin the first chapter, state-of-the art is presented for the synthesis, characterization and application of 2D materials. This chapter was organized in three subchapters: Heterogeneous photocatalysts, Semiconductor photocatalysts and Energy sources and utilization: What does the future hold?. The second chapter describes the materials and methods. In this chapter, the synthesis of several materials is presented as well as the characterization techniques and the photocatalytic experimental runs. The last experimental section consists in the presentation and discussion of the results. This chapter is divided into three sub-chapters: Synthesis of the

materials, Physical chemical properties of the materials and Solar fuels production, following a logical structure from fabrication to application. It is worth noting that, the primary purpose of the presented work is the preparation and characterization of materials, so in that sense, the selected application can be regarded as a mean of characterization of the photocatalyst activity, rather than a chemical engineering application.

2 Material synthesis and characterization: State of the art

2.1 Heterogenous photocatalysts

An optical semiconductor (SC), when used as a photocatalyst, is a material that can promote some reactions, by increasing their rate, using light as a source of activation. When an SC absorbs photons with energy higher than that of the band gap (E_{bg}), electrons populate the conduction band (CB) of the material while generated holes remain in the valence band (VB)[8]. These electron-hole pairs are referred to charge-carriers, because these are the species that promote the reduction-oxidation reactions. In the VB, the excess of holes promotes the oxidation reactions while in the CB, the electrons promote reduction reactions[8,9]. A schematic representation of an operative optical semiconductor can be seen in Figure 1.

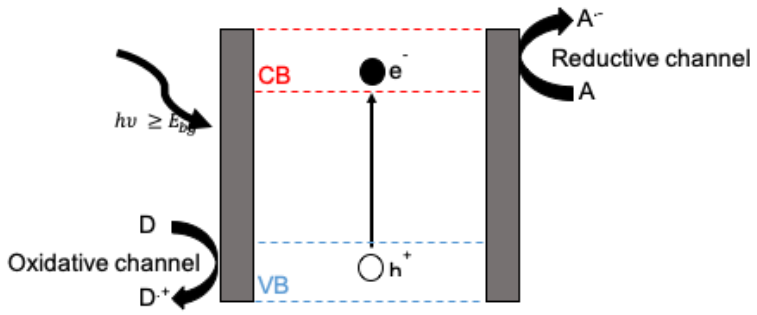

Figure 1 - General representation of a semiconductor.

The knowledge of the positioning of the VB, the CB and the value of E_{bg} is vital for photocatalysis, to understand and predict if our catalyst is suitable for an application[10-12].

In 1966, Tauc proposed a method to determinate the E_{bg} in which required the optical absorption spectra of the semiconductor material[13]. However, nowadays, the E_{bg} is usually estimated by the diffuse reflectance spectra, applying the Kubelka-Munk units[14]. Briefly, in this method, a line is drawn/fitted, in the linear region of increasing intensity in the diffuse reflectance spectra with Kubelka-Munk units. The intersection of this line and the X-axis gives an estimation of the E_{bg}[14]. This method is quite useful, mainly due to its simplicity and quickness in obtaining results. Nevertheless, the process is not accurate if the material shows a considerable absorption at energies below the E_{bg}[14].

For a semiconductor to be suitable for the photocatalytic production of H_2 molecular, or the photoreduction of CO_2, either, its CB should be more negative than the potential required for the formation of the corresponding CO_2 photoreduction products, or, correspondingly, the VB should be more positive than potential for the oxidation of water, to produce hydrogen[10,11].

Figure 2 shows the positions of the VB and CB, band gap energy and redox potentials values for some types of semiconductors.

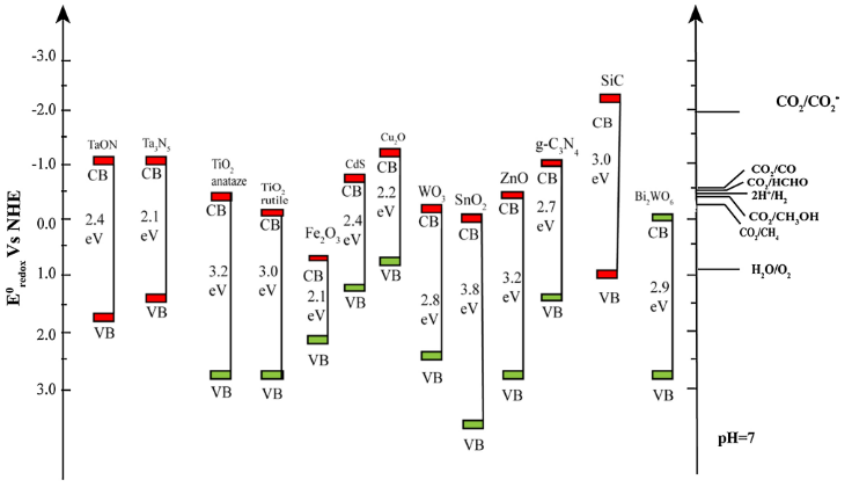

Figure 2 - Valence band (VB), conduction band (CB), band gap energy (E_{bg}) and potential (E^o) values for some semiconductors. The potential values required to carry out CO_2 reduction and H_2 production are also indicated on the right axis-side. Reprinted from [10].

One of the most studied and applied photocatalysts is, by far, TiO_2, mainly due to its low cost, reduced toxicity and good resistance[15-17]. As shown in Figure 2, its CB and VB positions are suitable for both CO_2 photoreduction and H_2 production. However, this semiconductor, like many others, has some limitations, such as high recombination of the charge-carriers and low absorption of light in the visible region (E_{bg}= 3.0-3.2 eV), which decreases the photocatalytic efficiency for the production of solar fuels[18-20]. The development of new inexpensive materials that are selective towards the generation of H_2 or the reduction of CO_2 with high efficiency is a key goal within this subject[21].

For instance, graphitic carbon nitride (g-C_3N_4, or simply GCN) with a band gap energy of 2.7 eV presents enhanced absorption in the visible region compared to TiO_2. Also, because of the position of its CB, which is more negative than the potential for the reduction of CO_2, and its VB more positive than the oxidation of water[22], it is a good candidate for photocatalytic H_2 production and CO_2 photoreduction. Nevertheless, among other limitations, it still presents limited visible light absorption.

To overcome some of these and other limitations, several pieces of research focused on carbon-based materials (carbon nanotubes, graphitic carbon nitride, graphene and others), either to couple with other type of semiconductors or to act alone as photocatalysts[16,23]. Several authors suggest that creating a composite with a carbon material can improve the photocatalytic activity, due to an inhibition of the recombination of the charge carriers[20,24,25].

2.2 Semiconductor photocatalysts

2.2.1 Graphitic carbon nitride

One promising 2D semiconductor photocatalyst that has grasped the attention of researchers worldwide is graphitic carbon nitride[6,20]. This material has significant advantages such as facile and economic preparation, some absorption in the visible region (E_{bg} = 2.7 eV), suitable potentials to carry out H_2 production and CO_2 reduction and good chemical stability[6,18,26].

There are several routes to prepare this material. The most common, simple and less expensive way is the thermal polymerization of precursors rich in carbon and nitrogen, such as urea, dicyandiamide, melamine and others[6,26,27]. However, other methods are used to prepare GCN, like supramolecular assembly, or rapid microwaved assisted, but these might be cost-demanding and time-consuming[6]. Nevertheless, synthesizing GCN from different precursors has a significant influence in the optical and electronic properties of the final material, showing differences in the surface area, porosity and other surface properties, that directly influences the photocatalytic activity[19,21].

A proposed chemical structure for polymeric GCN is shown in Figure 3. The C-N bonds in the layer of GCN and the NH_2 molecules at the edges of each sheet of carbon nitride are evident in this illustration.

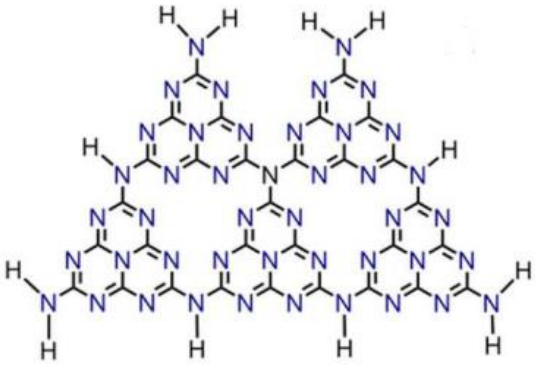

Figure 3 - Proposed structure for bulk graphitic carbon nitride. Reprinted from [28].

Nevertheless, bulk GCN has some limitations such has a low surface area, high recombination of the charge-carriers and a wide band gap (2.7 eV)[7,19,24]. Therefore, tremendous efforts are in course to overcome these restrictions by performing several types of modifications to the bulk material. One of the processes consists in performing chemical, mechanical or thermal treatments[26,29]. Other strategies consist in doping metals and non-metals to improve its photoactivity or in coupling it with another semiconductor material to form heterojunctions[30,31].

While mechanical exfoliation seems a good approach to modify bulk GCN, it usually generates low yields of material, and thus the scale-up of this method is not interesting[32]. Also, the surface area of the resulting material is not considerably changed by mechanical treatments[26].

Thermal treatments have also been performed to exfoliate the bulk material, increasing the space between sheets, thus creating a material less dense and with a higher surface area[32]. Lima *et al.* reported the influence of temperature in the bulk exfoliation of carbon nitride prepared form dicyandiamide, concluding that a temperature of 500 ºC is the ideal temperature, creating a good compromise between the yield of material and a decent exfoliation[26]. However, a combination between a thermal treatment and a mechanical treatment can be an interesting pathway towards modifying carbon nitride efficiently, with proper photocatalytic activity[33].

The deposition of a metal in GCN, to act as a co-catalyst, can also enhance the photoactivity of the material, by creating a synergistic effect between the carbon phase and the metal. Several metals have been deposited in carbon nitride, such as copper, gold, platinum, ruthenium, and others[34-36].

There is also an influence on doping non-metals in the surface of GCN. Several non-metals were deposited in carbon nitride, as a modification to improve its photo-efficiency. Some of the reported non-metals include carbon, phosphorus and oxygen[37,38]. Doping phosphorus can indeed narrow the band gap of the material, promote the separation between the charge-carriers and increase the absorption of visible-light, thus enhancing the photocatalytic activity[39].

2.2.2 Graphene oxide

Since the discovery of graphene in 2004, this material has seized the attention of researchers worldwide. Graphene, another 2D carbon material, being a single sheet of carbon with sp^2 bonds, has unique and extraordinary properties such has a high specific surface area and a high electronic conductivity[4,16,40]. The production of graphene from graphite has evolved over the past years since the mechanical exfoliation by the scotch tape method[18]. With several methods, such as a more recent mechanical exfoliation or supported growth on substracts by chemical vapor deposition, graphene production is nowadays an easier task than in the past decades[18,40].

Another material based in graphene, graphene oxide (GO), is normally obtained by treating graphite with acids[15]. This material differs from graphene by having oxygen groups on its surface and edges, allowing covalent and non-covalent interactions with other molecules, and also working as anchoring sites[15,23,41]. The chemical oxidation of graphene is, usually, the most straight-forward method to prepare GO, due to its simplicity and capability of production in large scales[18].

The most popular method to produce GO is the Hummers method or its modified form, due to its simplicity[41]. Nevertheless, other methods are also common, such as the Brodies or Tours method[41]. The original Hummers method produces GO by adding a mixture of potassium

permanganate, concentrated sulfuric acid and sodium nitrate to graphite, in a bath at 0 ºC, performed in some steps, for safety reasons[18,41,42].

After the chemical exfoliation/oxidation of graphite into GO, this material can be reduced to reduced graphene oxide (rGO)[18]. The rGO material is similar to GO. However, the oxygen groups in its surface are mainly hydroxyl type. Nevertheless, the coupling of GO with other materials should be performed before the reduction of GO, because a large number of oxide groups can facilitate this coupling[18].

A representation of rGO can be seen in Figure 4. A single sheet of rGO is presented, with the reduced oxygen species on its surface, consisting of mainly hydroxyls and epoxy groups.

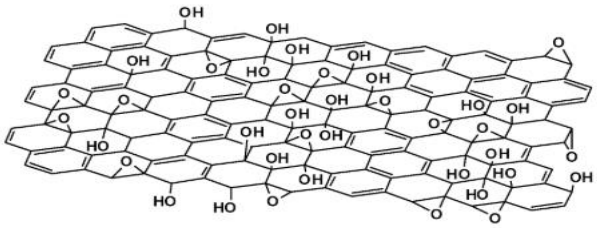

Figure 4 - Representation of a sheet of reduced graphene oxide. Reprinted from [41].

GO alone can act as a photocatalyst and, in particular, produce solar fuels. However, it has a weaker performance than other photocatalysts[15]. Therefore, several researchers have focused their attention on improving the photocatalytic activity of GO and rGO.

The tuning of the oxidation degree of GO can be changed by varying the amount of potassium permanganate, resulting in materials with different properties, in particular, different band gap energies[18]. Another important surface property is the number of defects present in the structure of GO, that leads to a higher conductivity. Reported rGO with fewer defects has shown a higher photocatalytic activity than bare rGO[18].

Many pieces of research have been conducted on coupling GO with metal oxides and metal sulphides, mainly TiO_2 and CdS, which could enhance the optical and photocatalytic properties of the resulting material[43]. When a composite of TiO_2 and rGO is created, a significant enhancement of the photocatalytic activity is observed, due to synergetic interaction between the two materials, leading to efficient electron transfer and charge separation[23].

2.2.3 Molybdenum disulfide

Molybdenum disulfide (MoS_2) is an important material within photocatalysis. Its graphitic form, being a quasi-2D material, has van der Waals interactions between different layers while having strong covalent forces between atoms within one layer[5,44]. Due to its high surface area, it is an interesting material in several different applications such as catalysis, nanoelectronics and sensors[7].

In a 3D computer generated structure for MoS_2, it is possible to observe the almost pristine planar (2D) structure of this material (Figure 5).

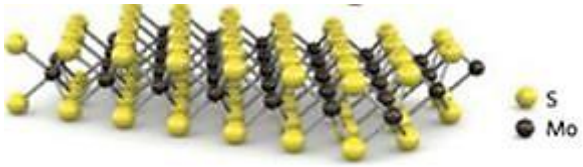

Figure 5 - 3D structure for MoS_2, adapted from [45].

There are several routes to prepare MoS_2 with significant differences in the final material. Studies report that the most common method for photocatalytic purposes is the hydrothermal synthesis in an autoclave, at high temperatures and pressures, with molybdenum and sulphur precursors. By this synthesis, ultrathin nanosheets of MoS_2 can be produced[46].

Nevertheless, modifications to MoS_2 have been studied to improve its properties and photocatalytic activity, with the chemical exfoliation playing an important role[46]. The chemical exfoliation by the solvent-based exfoliation produces 2D layers of MoS_2 flakes suspended in a solution. Briefly, in this method, a mixture of MoS_2 and an organic solvent is ultrasonicated for some time to decrease the interactions between different layers of MoS_2[46].

MoS_2 can act efficiently as a co-catalyst due to improving the optical properties, by increasing light harvesting, and promoting charge separation, thus improving the photocatalytic activity[7]. This material could be a good approach towards replacing noble metals (such as Pt) as co-catalysts in photocatalysis, decreasing the overall cost of production and being a more sustainable production of efficient photocatalysts[5,47].

Therefore, reports on graphitic carbon nitride and MoS_2 as a co-catalysts show that these materials form an interesting composite, with a good network and interaction between them, with the formation of a heterojunction, that can improve light harvesting and promote the separation of the charge-carriers within the material[5,7].

MoS_2 can also be a suitable co-catalyst for rGO. Studies shows that the composite between MoS_2 and rGO exhibits a superior photocatalytic activity, comparing with MoS_2 bare. These results are explained by higher absorption of light and lower recombination of the charge- carriers, increasing the overall photoefficiency[48,49].

2.2.4 Other materials

2.2.4.1 Layered double hydroxides as photocatalysts

Layered double hydroxides (LDHs), commonly known as hydrotalcite, are 2D lamellar structures, natural or synthetic, composed by a positively charged brucite-like host layers with anionic species and water in the interlayer so that the overall charge be maintained[50-52]. Since

the discovery of these materials in Sweden, around 1842, they have been applied in catalysis and adsorption, due to their low cost of production, versatility and simplicity[53,54]. The general formula of LDHs is:

$$[M_{1-x}^{2+}\, M_x^{3+}\, (OH)_2](A^{n-})_{x/n}\, .mH_2O$$

where M^{2+} is a divalent metal (e.g., Mg^{2+}, Ni^{2+}, Cu^{2+}), M^{3+} is a trivalent metal (e.g., Al^{3+}, Fe^{3+}), A^{n-} is the interlayer anion (e.g., Cl^- CO_3^{2-}, NO_3^-) of valence *n* and *x* represents the molar ratio[51,55,56].

The general representation of an LDH is given in Figure 6, in which the interlayer is composed of carbonate anions and water molecules[54].

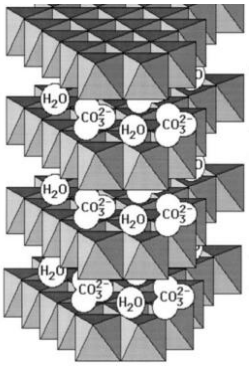

Figure 6 – Schematic representation of an LDH with carbonate ions and water in the interlayer. Reprinted from [54].

LDHs can be synthesized by several different methods depending on the properties or specifics desirable. These methods include precipitation at constant pH (co-precipitation) or increasing pH, hydrolysis reaction and anion exchange[53]. However, the most common method to produce LDHs is the co-precipitation, where the metal cations simultaneously co-precipitate, in an alkaline media or at increasing pH[53,57]. In this synthesis, the pH value is crucial, as it affects the chemical and structural properties of the LDH. It shouldn't be too low, because some salts may not precipitate and it shouldn't be too high to prevent the dissolution of one or more metal ions [53]. In alkaline media, a pH around 10 is used to prepare these materials[57]. In increasing pH, generally, a solution of NaOH is added to the mixture to induce the precipitation[58]. LDHs have been used as a support for catalyst, but their photocatalytic activity *per se* has been neglected for several years[52]. They show photocatalytic activity for the degradation of some organic pollutants and the production of O_2 through photocatalytic/photoelectrochemical water splitting[51,52].

These materials are also very relevant in CO_2 capture and storage, being interesting for the photocatalytic reduction of CO_2, owing to their sorption capability for CO_2 and their easily tuned properties[4].

2.3 Energy sources and utilization: What does the future hold?

Since the discovery of fire, humankind in its early days has evolved and revolutionized the energy consumption and utilization. With the increasing industrialization and life conditions (particularly since the mid-XIX century), the demand for energy has increased, with fossil fuels playing a key role in its sources[3].

Since the early '90s, energy consumption worldwide increased by around 60%, as shown in Figure 7. Renewable sources have been increasing in amount, but their exploitation and use are still minimal. In fact, fossil fuels (oil, gas and coal) correspond to around 85% of the total energy utilized. This value is confirmed by International Energy Agency, in 2017, that stated that 81.4% of the total consumed energy derived from natural gas, coal and oil[59]. These sources are the most widely used since the dawn of the industrial revolution.

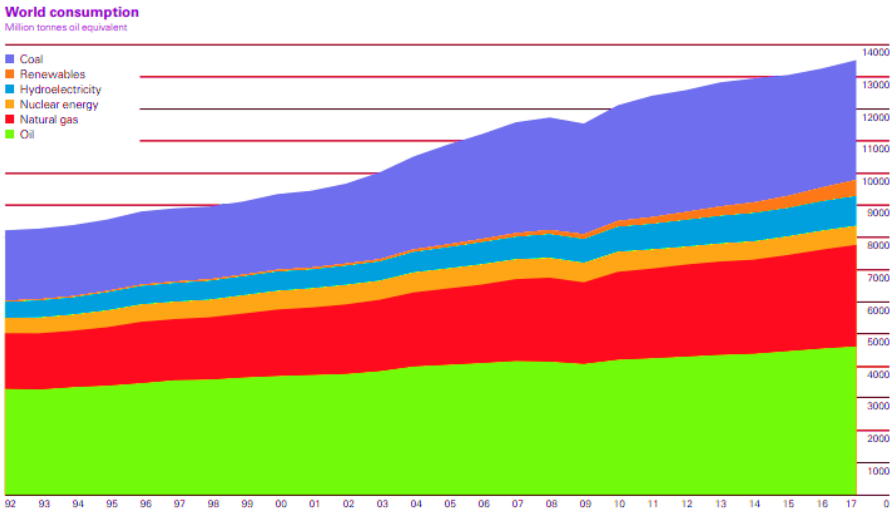

Figure 7 - World energy consumption since 1992, in millions of tons of oil equivalent. Reprinted from [60].

However, it is unrealistic to imagine and develop a new energy economy without the usage of fossil fuels shortly because our whole society is dependent on these sources. Since these sources became scarcer and more difficult to access, new prospects have appeared in the future of energy.

Carbon dioxide emissions increased around 1.7%, which indicates that the exploitation of fossil sources increased and that renewable sources are not yet capable of sustain modern society[60]. Other studies report that the concentration of CO_2 in the atmosphere has increased around 31% over the past 200 years, proving in fact that this rise in CO_2 is caused by human life[3].

So, new technologies in energy must be developed to slow/reverse the amount of CO_2 emissions[2]. Several routes are considered to be a two-in-one approach (kill two birds with one stone) such as the photochemical, electrochemical, photoelectrochemical or biological

reduction of CO_2 into solar fuels[61]. By one hand, CO_2 is used as a carbon feedstock to produce fuels and, in other, the amount of CO_2 in the atmosphere decreases[10,31].

The scientific community, in general, has embraced the reduction of CO_2 into fuels and the production of other solar fuels, such as hydrogen, towards a more sustainable society[10,20,62-64].

2.3.1 Solar Fuels

2.3.1.1. Photocatalytic hydrogen production

Another potential source to have in account is hydrogen since it is abundant and its combustion releases only water[59]. There are several routes to hydrogen production. Hydrogen can be produced by thermal reforming of CO_2, where CO_2 reacts with CH_4 producing hydrogen and carbon monoxide[3]. However, this process requires a high input of energy and high temperatures, which are not particularly good conditions to catalysts as they can easily be deactivated or inutilized[3]. Having these conditions in mind, the photocatalytic production of hydrogen has appeared as a green technology, inspired by the natural photosynthesis, capable of transforming solar energy into solar fuels, from renewable sources such as aqueous (water splitting) or organic wastes[28,65,66].

Nevertheless, there are some problems inherent to the photocatalytic production of hydrogen, with the use of inefficient and non-selective photocatalysts being the most problematic issues, in particular, with the rapid recombination of the charge-carriers[18].

The deposition of metals in several photocatalysts, to act as co-catalysts, has proven to be a valid route to promote hydrogen production[66]. However, the use of noble metals is expensive, and its extraction is scarce, so, new ways of boosting hydrogen production must be developed[67]. Non-metal doping, such as carbon, phosphorus, oxygen and selenium doping appears to have a tremendous potential[38,68].

In Table 1 are listed some types of photocatalysts applied for the photoproduction of hydrogen.

Table 1 – List of photocatalysts reported for the production of hydrogen.

Photocatalyst	Precursor and synthesis	Photocatalytic experiments	Results	Ref.
M-tetrakis (*m*-carboxyphenyl) porphyrin/GCN	Calcination of dicyandiamide and impregnation	150 W Hg lamp with a cutoff filter for UV light EDTA as a sacrificial agent	2224 $\mu mol \cdot g^{-1} \cdot h^{-1}$ of H_2	28
Pt/GCN	Calcination of dicyandiamide and a post thermal treatment	350 W Xe lamp with a cutoff filter for UV light TEOA as a sacrificial agent	1220 $\mu mol \cdot g^{-1} \cdot h^{-1}$ of H_2	35
Pt (C doped GCN)	Calcination of melamine	100 W Xe lamp with a cutoff filter for UV light TEOA as a sacrificial agent	1889 $\mu mol \cdot g^{-1} \cdot h^{-1}$ of H_2	68
Pt (Mo doped GCN)	Calcination of melamine	300 W Xe lamp with a cutoff filter for UV light TEOA as a sacrificial agent	2009 $\mu mol \cdot g^{-1} \cdot h^{-1}$ of H_2	65
MoS_2/GCN	Calcination of cyandiamide and impregnation of MoS_2	300 W Xe lamp with a cutoff filter for UV light Lactic acid as a sacrificial agent	1030 $\mu mol \cdot g^{-1} \cdot h^{-1}$ of H_2	5
CdS/GO	Impregnation of CdS nanoparticles in GO	4 LEDs of 4 W each (λ= 450)	8666 $\mu mol \cdot g^{-1} \cdot h^{-1}$ of H_2	59
1 % CdS/NiS/rGO	Modified Hummers method with impregnation of CdS in NiS/rGO	300 W Xe lamp with a UV cutoff filter 30 % (v/v) of lactic acid	1496 $\mu mol \cdot g^{-1} \cdot h^{-1}$ of H_2	69
TiO_2/GO	Tour's modified method	250 W metal halide lamp 30 % (v/v) of methanol	6500 $\mu mol \cdot g^{-1} \cdot h^{-1}$ of H_2	70
$NiTiO_3$/rGO	Modified Hummers method	100 W halogen lamp 5 % (v/v) of methanol	8383 $\mu mol \cdot g^{-1} \cdot h^{-1}$ of H_2	64
ZnS-ZnO/Zn-Al LDH	Solvothermal method at pH 12 (constant)	Hg lamp with a wavelength of 254 nm	1599 $\mu mol \cdot g^{-1} \cdot h^{-1}$ of H_2	71
gCN/Zn-Cr LDH	Coprecipitation of metal precursors at constant pH (pH=5.5) and calcination of melamine	300 W Xe lamp 10% (v/v) of TEOA and 1% of Pt nanoparticles	187 $\mu mol \cdot g^{-1} \cdot h^{-1}$ of H_2	72

2.3.1.2. Photocatalytic CO_2 reduction into fuels

The principles of photocatalytic reduction of CO_2 into solar fuels can be resumed as in Figure 8. In summary, CO_2 can be reduced by solar energy to produce fuels, such as methanol or ethanol. The combustion of these solar fuels produces energy, which can be used for different applications. As any combustion, it releases water vapor and CO_2, closing this renewable cycle.

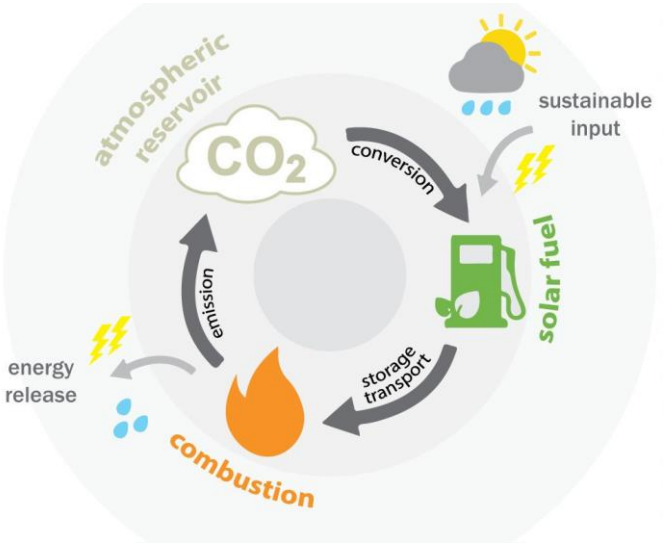

Figure 8 - Overview of the photocatalytic reduction of CO_2. Reprinted from [73].

The major products produced by the photocatalytic reduction of CO_2 differ according to the different reaction conditions. Usually, these products are methanol, ethanol, formic acid, carbon monoxide and methane[18,19,29,74,75].

However, there are some problems inherent to the photocatalytic CO_2 reduction. One of them is that most semiconductor materials/photocatalysts are not efficient and not stable, as so in the photocatalytic production of hydrogen[1]. Also, the design of new photocatalyst that does not use metals is of great interest, due to an economic point of view and to the sustainability of those metal resources[1]. Therefore, the designing of efficient and CO_2 selective catalysts is of great importance to improve the overall efficiency of the process.

Table 2 lists some examples of photocatalysts used for the production of fuels by the photocatalytic reduction of CO_2.

Table 2 - List of photocatalysts used for the production of solar fuels by photoreduction of CO_2.

Photocatalyst	Precursor and synthesis	Photocatalytic experiments	Results	Ref.
GCN	Calcination of urea	300 W Xe lamp with a cutoff filter for visible light (λ ≥ 420 nm)	6.28 μmol·g^{-1}·h^{-1} of MeOH 4.51 μmol·g^{-1}·h^{-1} of EtOH	21
GCN	Calcination of melamine	300 W Xe lamp with a cutoff filter for visible light (λ ≥ 420 nm)	3.64 μmol·g^{-1}·h^{-1} of EtOH	21
2.5 % Cu-TiO_2/GCN	Calcination of urea	300 W Xe lamp with a cutoff filter for visible light (λ ≥ 400 nm)	22.3 μmol·g^{-1}·h^{-1} of CH_4	20
ZnO/GCN	Calcination of urea	500 W Xe lamp with a cutoff filter for UV light (λ ≤ 420 nm)	38.7 μmol·g^{-1}·h^{-1} of CO 19.0 μmol·g^{-1}·h^{-1} of MeOH	24
MoS_2/GCN	Calcination of urea	500 W Xe-arc immersion lamp	8.37 μmol·g^{-1}·h^{-1} of CO	76
0.5% Pt/GCN	Calcination of urea	300 W Xe lamp with a cutoff filter for visible light (λ ≥ 420 nm) Methanol as a solvent	4.5 μmol·g^{-1}·h^{-1} of CO 1.8 μmol·g^{-1}·h^{-1} of CH_4	36
GO	Modified Hummers method with acid treatment	300 W halogen lamp	0.172 μmol·g^{-1}·h^{-1} of MeOH	15
TiO_2/GO	Modified Hummers method	UV-Vis medium-pressure mercury immersion lamp	12.5 μmol·g^{-1}·h^{-1} of MeOH 144.7 μmol·g^{-1}·h^{-1} of EtOH	77
CdS/rGO (0.5% rGO)	Modified Hummers and a microwave hydrothermal method	300 W Xe immersion lamp with a cutoff filter for UV light	2.51 μmol·g^{-1}·h^{-1} of CH_4	25
TiO_2/rGO (0.4% rGO)	Tour's modified method	500 W Hg lamp with H_2O as a reductant agent in the gas phase	12.75 μmol·g^{-1}·h^{-1} of CH_4 11.93 μmol·g^{-1}·h^{-1} of CO	78
Ni-Al LDH (Cl^-)	Coprecipitation of metal precursors at pH 10 (constant)	400 W Hg lamp	4.2 μmol·g^{-1}·h^{-1} of CO 2.46 μmol·g^{-1}·h^{-1} of H_2	79
Mg-In LDH	Coprecipitation of metal precursors at pH 10 (constant)	200 W Hg-Xe lamp	3.21 μmol·g^{-1}·h^{-1} of CO 17.0 μmol·g^{-1}·h^{-1} of O_2	51

3 Materials and Methods

3.1 Synthesis of graphitic carbon nitride materials

Bulk graphitic carbon nitride was synthesized by thermal decomposition of dicyandiamide. Briefly, 2 g of dicyandiamide was placed in a semi-closed crucible within a muffle, in an air atmosphere. The equipment was set to heat up to 450 ºC, at a rate of 2 ºC·min^{-1}, followed by maintaining that temperature for 2h. Then, another ramp up to 550 ºC, at a rate of 2 ºC·min^{-1} was performed and maintained that temperature for 4h[26]. After the thermal decomposition, the resultant yellow powder was ground, washed with ultrapure water and dried overnight in an oven at 100 ºC. This material is from now on designated as GCN.

Subsequently, a thermal treatment was performed to this material to obtain nanosheets. Briefly, 1.2 g of GCN was placed in a rectangular crucible in a muffle, in an air atmosphere. The equipment was set to heat up to 500 ºC, at a rate of 2 ºC·min^{-1}, and maintained that temperature for 2h[26]. This material was abbreviated as GCN(T), where T stands for thermal treatment.

3.1.1 Synthesis of metal-doped graphitic carbon nitride

Several noble metals (Au, Pd, Pt and Ru) were impregnated in GCN and GCN(T), as described below.

Firstly, a certain amount of the precursor of each metal (see Appendix A) was dissolved in 1 mL of distilled water and added, drop-by-drop, to 1 g of GCN or GCN(T), to obtain 1.0 wt% of metal, except for the Pd composite, in which water was replaced by concentrated hydrochloric acid. The mixture was then sonicated for 90 minutes and dried at 60 ºC overnight. Afterwards, the materials were treated in an oven, with a flow of 50 mL·min^{-1} of N_2, for 1h at 200 ºC for Au, Pd and Pt and at 350 ºC for Ru, followed by a reduction with a flow of 50 mL·min^{-1} of H_2 for 3h, at the previous set temperature. Finally, the materials were ground to obtain a homogeneous mixture. These materials were designated as GCNM and GCN(T)M, where M represents the metal that is doped in carbon nitride.

3.1.2 Synthesis of non-metal doped graphitic carbon nitride

The non-metal doped carbon nitride was prepared with phosphorus (P) and phosphorus-oxygen (PO). These composites were synthesized by thermal decomposition of dicyandiamide in the presence of a precursor of the non-metal.

In brief, to prepare P-doped GCN, 2 g of dicyandiamide was placed in a semi-closed crucible in a muffle, with a certain amount of 2-aminoethlyphosphonic acid, to obtain 1.0 wt% of P in GCN.

Then the equipment was set with the same temperature ramps as GCN (described in Section 3.1). The final material was then washed with water and left to dry overnight in an oven at 60 ºC. The resulting material was designated as GCNP, where P stands for phosphorus.

To prepare the P and O doped GCN, the procedure was the same as before, but a certain amount of citric acid was also added to the crucible, before the thermal decomposition. The resulting material was designated as GCNPO, where P stands for phosphorus and O for oxygen.

3.2 Synthesis of molybdenum disulfide

Molybdenum disulfide was synthesized by a one-step reaction of a mixture of potassium thiocyanate (KSCN) and molybdenum trioxide (MoO_3)[7]. Briefly, 1.45 g of KSCN and 0.86 g of MoO_3 were each dissolved in 20 mL of distilled water. Afterwards, both aqueous solutions were mixed and added more 20 mL of water. This solution was left agitating for around 30 minutes, before hydrothermal treatment in a Teflon-lined autoclave at 180 ºC for 24h.

The obtained black material was centrifuged, washed several times with distilled water and dried overnight in an oven at 60 ºC. This material was designated as MoS_2 (abbreviated as M).

3.3 Synthesis of molybdenum disulfide/graphitic carbon nitride composites

Several composites, with different percentages of MoS_2 and with two types of graphitic carbon nitride (thermal exfoliated and non-metal doped), were prepared by two different routes: impregnation (abbreviated as I) and preparation *in-situ* in an autoclave (abbreviated as A).

3.3.1 Impregnation method

Two composites were prepared by this route using 1.0 wt% and 2.5 wt% of MoS_2 in GCN(T).

Briefly, a certain amount of GCN(T) and MoS_2 was mixed in 30 mL of ethanol (EtOH) and left agitating for 2h. Afterwards, this mixture was left in ultrasound for another 2h. Subsequently, the mixture was centrifuged and washed several times with EtOH. The resulting powder was then left in an oven overnight, to dry, at 60 ºC. The materials were designated as GCN(T)M1.0I and GCN(T)M2.5I.

3.3.2 *In-situ* method

Three sets of materials were prepared by this method: GCN(T) with 1.0 wt% of MoS_2, and GCNP and GCNPO with 1.0 wt% of MoS_2.

Briefly, a certain amount of graphitic carbon nitride materials (GCN(T), GCNP and GCNPO) and of MoS_2 (1.0 and 2.5 wt%) were mixed in 30 mL of ethylene glycol and left agitating for 30 minutes. Then 30 mL of ethylene glycol was added to the mixture and this solution was subjected to a solvothermal treatment in a Teflon-lined autoclave at 180 ºC for 12h. Finally, the mixture was centrifuged and washed several times with EtOH. The materials were put to dry overnight in on oven at 60 ºC.
The three composites prepared by this route were designated as GCN(T)M1.0A, GCNPM1.0A and GCNPOM1.0A.

3.4 Synthesis of reduced graphene oxide materials

The synthesis of the materials described in this section was performed by Doctor Luísa Maria Pastrana-Martinez from University of Granada (Spain).

Graphene oxide was prepared from commercial graphite, using the modified Hummers method, described in detail elsewhere[23]. Briefly, 360 mL of concentrated sulfuric acid, 7.5 g of sodium nitrate and 45 g of potassium permanganate were used to prepare a graphene oxide suspension. After sonication and centrifugation, the suspension was reduced to produce reduced graphene oxide and designated as rGO.

3.4.1 Synthesis of reduced graphene oxide/MoS_2 composites

The materials were prepared following a simple hydrothermal method. In a typical synthesis, an amount of sodium molybdate and thiourea (molar ratio = 1:7) were added to water, and then, the mixture was transferred into a Teflon-lined stainless-steel autoclave, which was heated at 200 ºC for 24h. After that, the black solid was collected and washed with water and dried in an oven at 80 ºC for 24h. The composite with graphene oxide was obtained by replacing water with an appropriate amount of aqueous GO solution (1.0 $g \cdot L^{-1}$). These materials were designated as GOMx, where x is the wt% of MoS_2 in rGO.

3.5 Synthesis of platinum nanoparticles suspension

When necessary, platinum (Pt) nanoparticles were used as co-catalyst in some of the photocatalytic hydrogen experiments. Briefly, an aqueous solution of dihydrogen hexachloroplatinate (IV) hexahydrate (60 mg in 20 mL of water) was added, drop-by-drop, to a methanol solution containing L-ascorbic acid (600 mg in 180 mL of methanol). Afterwards, the mixture was heated and stirred, under reflux, during 3h. The suspension was centrifuged, after

cooling, and the solid was washed several times with methanol. Afterwards, the solid was resuspended in a given volume of water to obtain aqueous Pt nanoparticles[37].

3.6 Catalysts characterization

The instruments used to characterize the synthesized materials are described in Appendix B.

The optical properties of the material were studied by diffuse reflectance UV-Vis spectroscopy. Since light cannot penetrate opaque (solid) samples, it is reflected on the surfaces. The incident light scattered in different directions is called diffuse reflection. With integrating spheres, measurement is performed by placing the sample in front of the incident light and concentrating the light reflected from the sample on the detector using a sphere with a barium sulfate-coated inside. The obtained value becomes the reflectance (relative reflectance) concerning the reflectance of the reference standard, which is taken to be 100%. The obtained distribution can be converted in absorption spectra, which reflect the electronic transitions obtained upon absorption of energy in the form of ultraviolet light or visible light.

The adsorption-desorption isotherms were performed to study the surface of the materials. Briefly, materials can adsorb molecules of gas in its surface. Adsorption and desorption are carried at constant temperature (isotherms), usually 77 K with N_2 liquid. The amount of adsorbed molecules is extracted in terms of the relative pressure of the gas. After the adsorption-desorption results, the surface area of the material can be calculated by the BET equation (Brunauer-Emmett-Teller)[80].

Photoluminescence spectroscopy (PL) was used to probe the electronic structure of materials. Light is directed onto a sample, where it is absorbed and imparts excess energy into the material in a process called photo-excitation. One way this excess energy can be dissipated by the sample is through the emission of light, or luminescence. In the case of photo-excitation, this luminescence is called photoluminescence. Photo-excitation causes electrons within a material to move into permissible excited states. When these electrons return to their equilibrium states, the excess energy is released and may include the emission of light (a radiative process) or may not (a nonradiative process). The energy of the emitted light (photoluminescence) relates to the difference in energy levels between the two electronic states involved in the transition between the excited state and the equilibrium state. The quantity of the emitted light is proportional to the relative contribution of the radiative process[35].

X-Ray diffraction (XRD) was also performed. X-rays have wavelengths in angstrom dimensions and have sufficient intensity to penetrate materials. In XRD analysis, the crystallinity of the material causes the diffraction of the beam of X-ray into various angles. The existence of aligned and well-orientated molecules (definition of crystallinity) originates well defined peaks in the pattern of XRD of the material[81]. With the angle of the defined peaks, by using Bragg relation, we can estimate the lattice spacing, which is characteristic to one material. An X-ray analysis could also give an indication of metal particle size[81].

Scanning electron microscopy (SEM) was performed to better understand the morphology and aggregation state of the material. Briefly, a narrow beam of high intensity primary electrons is directed to the surface of the material and the backscattered or secondary electrons are detected as a function of the position of the primary beam. While the secondary electrons arise from the surface of the material, the backscattered electrons can penetrate into deeper regions of the sample. The contrast is due to the orientation of the electrons to the detector. Surfaces facing the detector will be closer and thus, appearing brighter in the image[81].

The deposition of metals and the morphology of metal loaded catalysts was studied through transmission electron microscopy (TEM). In TEM, a primary beam of electrons with high intensity and energy passes through a condenser, so the beams are parallel and pass through our sample. Then the transmitted electrons are detected and a 2D image is obtained[81].

Infra-red Fourier transformed-Attenuated total reflection (FTIR-ATR) was performed to better understand the bonds at the surface of the materials, with transmission as an indication of the intensity. The ATR crystal allows the penetration of the beams into the sample until 1-2 micrometers[81].

3.7 Photocatalytic runs

The photocatalytic runs for H_2 production from water splitting were carried out in a cylindric glass reactor, filled with 100 mL of an aqueous solution containing EDTA 0.2 $mol \cdot L^{-1}$ and 0.3 $g \cdot L^{-1}$ of catalyst. When the catalytic activity of the materials GCN, GCN(T), GCNP and GCNPO was tested, Pt nanoparticles (1.0 wt%) were added to 100 mL of aqueous solution containing EDTA 0.2 $mol \cdot L^{-1}$ (15% vol.) and 0.3 $g \cdot L^{-1}$ of catalyst, to boost the production of hydrogen.

The solutions were continuously purged with nitrogen to remove all oxygen and kept in the dark conditions for 30 min. The light source consisted of a system with 4 LEDs, with maximum emission at 423 nm, symmetrically around the glass reactor. The average nominal irradiance of each LED was 1000 $W \cdot m^{-2}$. After purging the solutions, the LEDs were turned on, and the reaction was carried out for 2h.

The amount of H_2 evolved was measured using an online gas chromatograph with argon as a carrier gas. Measurements were taken every 5 min during the 2h.

4 Results and discussion

4.1 Synthesis of the materials

Several types of 2D materials have been synthesized, characterized and its activity was evaluated towards the photocatalytic production of hydrogen. Bulk graphitic carbon nitride (GCN), molybdenum disulfide (MoS_2) and graphene were synthesized according to the reported methods and described in detail in Chapter 3. Modifications to GCN structure was performed by a thermal exfoliation at 500 ºC in air, by doping (metals and non-metals) and by preparing composites of carbon nitride with MoS_2 to obtain materials with improved absorption in visible and/or decreased recombination of charge-carriers. The same principle was applied to graphene composites with MoS_2.

The thermal polymerization of dicyandiamide into graphitic carbon nitride produced a bulk yellow powder (GCN), with a yield of 80%. One way to overcome the limited properties of GCN (see Chapter 2.2.1), is by forming nanosheets, which will produce materials with higher surface area and small particle size. Therefore, a thermal treatment was applied to GCN, giving rise to a light-yellow powder (GCN(T)), much less dense than the bulk material, with a yield of 35-40%. Both of these materials were doped with metals (Au, Pt, Pd and Ru) by a simple wet impregnation, followed by reduction in an oven using different temperatures. MoS_2 was prepared by a solvothermal method, in an autoclave, using potassium thiocyanate as S source and molybdenum trioxide as Mo source.

The formation of composites (or heterojunctions) is another way to overcome the limitations of carbon nitride, and therefore, two procedures were used to prepare composites of carbon nitride and MoS_2: i) impregnation and ii) *in-situ*, using an autoclave. As bare GCN(T) presents better properties than GCN, this material was chosen to prepare the composites. When preparing the composite of GCN(T) and MoS_2 by the autoclave method (GCN(T)M1.0A), a significant decrease in the obtained mass occurs, when comparing with the same material for the impregnation method (GCN(T)M1.0I). This is due to the higher temperatures and pressures within the autoclave as compared to the impregnation method, in which the mixture was carried out at room temperature.

Another synthesis strategy consisted in doping GCN with phosphorus and phosphorus-oxygen, *in-situ*, originating chemically modified carbon nitride (GCNP and GCNPO). This modification leads to a brown color powders, although slightly color differences were observed among each other.

The composites of reduced graphene oxide and MoS_2 (GOM), had no significant color changes between the different materials, mainly due to both the precursors (rGO and MoS_2) being black in color.

4.2 Physical chemical properties of the materials

The optical, electronic, textural, morphological and crystal properties of the materials were characterized by several techniques to obtain a relation between structure-photocatalytic activity.

4.2.1 Carbon nitride and metal doped carbon nitride

To study the influence of metal doping in carbon nitride and to compare the results with the published literature, several metals were doped in GCN and in GCN(T).

The optical properties of the materials were evaluated by UV-Vis diffuse reflectance spectroscopy (UV-Vis DRS). This is an important technique to assess the absorption of light of the photocatalysts and to estimate the band gap (E_{bg}) from the Tauc plots[14].

As shown in Figure 9a, both GCN and GCN(T) presents semiconductor-like absorption patterns in the blue region of the spectra, with the absorption maxima at approximately 370 nm attributed to the characteristic π–π* transitions owing to the heterocyclic aromatic system[37]. Moreover, the thermal exfoliation did not influence the presence of bands, although an increase in absorbance and a blue shift of the band edge is observed.

Another important characteristic of semiconductors is the photoluminescence (PL), as this gives an indication on the process of electron–hole migration, transfer and separation[55]. Normally, the higher the intensity of PL, the higher the amount of the recombined electron-hole. As displayed in Figure 9b, GCN presents the typical PL pattern of a semiconductor with an intense and broad fluorescence emission band with a maximum centered at 461 nm, a reflection of the high charge recombination caused by the π–π conjugated system of the graphitic-like structure[37]. For the GCN(T), the intensity of the emitted light increases when compared with GCN mainly due to the presence of fewer defects on the structure of the materials, which act as traps for the charge carriers, preventing their recombination[26]. Also, a blue-shit in the maximum wavelength occurs when exfoliating carbon nitride ascribed to the quantum confinement effect occurring in the material, due to the separation of layers and to the decrease of material size[26,82]. This blue-shift is consistent with the UV-Vis DRS results.

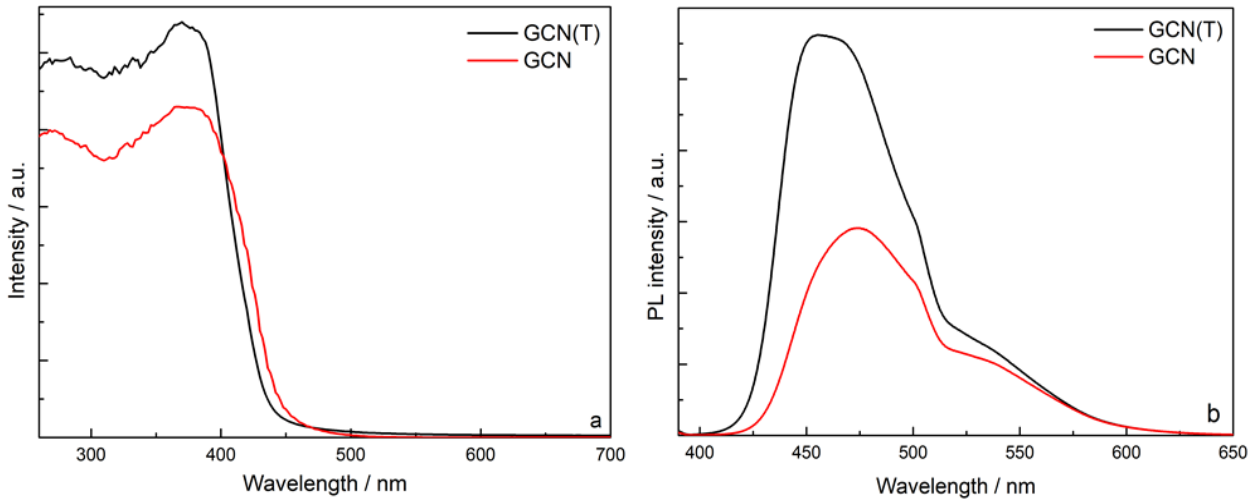

Figure 9 – UV-Vis DR spectra a) and PL spectra b) for GCN and GCN(T).

When loading metals (Pt, Pd, Ru, Au) in GCN and GCN(T) materials, several changes are observed in the UV-Vis absorption and emission spectra (Figures 10 and 11). Concerning the PL spectra (Figure 10), it is clear that the addition of a metal phase decreased the emission of PL intensity as compared to both GCN and GCN(T). Similar behavior was reported by Wang *et al.* in which the addition of Pt to carbon nitride decreased the intensity of the emitted light[36]. From all the doped materials, the ones containing Ru always have the lowest intensity of the emitted light, both in GCN and in GCN(T). Also, when adding a metal phase, a blue shift occurs in the maximum PL emission wavelength of both GCN and GCN(T), due to quantum size confinement.

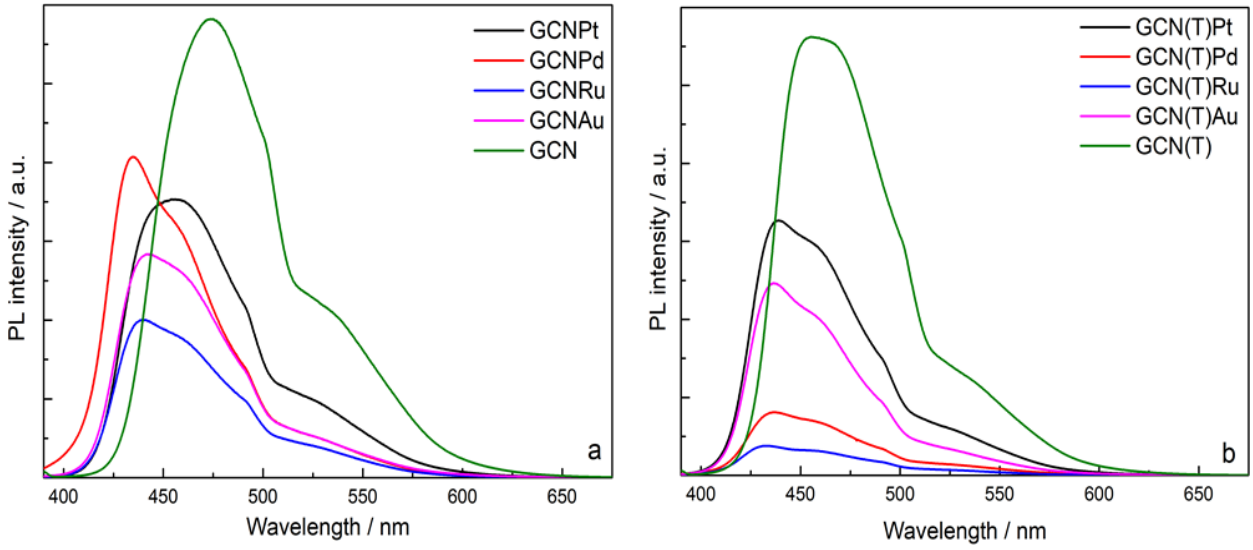

Figure 10 – PL spectra of a) GCN and b) GCN(T) doped with metals (Pt, Pd, Ru, Au).

In what concerns the UV-Vis absorption spectra, the addition of a metal phase to GCN and to GCN(T) increases the absorption of light in the visible range of the spectra, as displayed in Figure 11. These results are in agreement with the published literature[34]. The presence of Au nanoparticles in the composites show their typical plasmon band, with maximum peak at 550 nm. The Ru composite has always a higher absorbance than all other metals, probably due to its collor being darker than the other materials. Crossing this result of GCNRu and GCN(T)Ru with the PL spectra (which has the lowest intensity of all metal composites), a better photoactivity is expected for these materials.

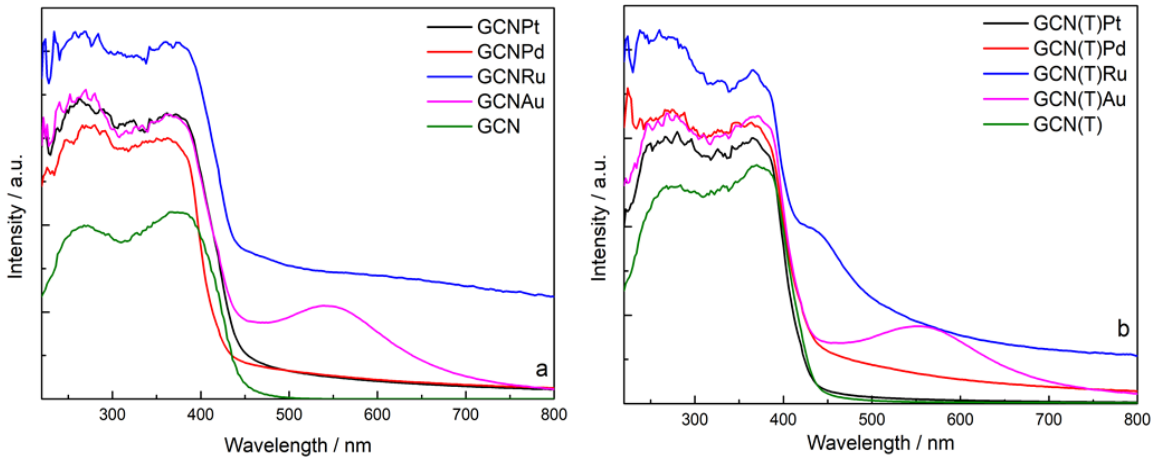

Figure 11 - UV-Vis DRS of a) GCN and b) GCN(T) materials doped with metals (Pt, Pd, Ru, Au).

An important characteristic of photocatalysts is the energy of band gap (E_{bg}) and its correct determination is crucial to perform a better screening of the appropriate materials for our applications. As so, the Tauc plots for undoped metal doped graphitic carbon nitride and doped with metals are presented in Figure 12, while Table 3 lists the E_{bg} for these materials, determined with and without a baseline correction.

From Figure 12 it is possible to observe that while GCN and GCN(T) have an intensity approximately zero for low energy values, the other materials tend to a certain value. So, when calculating the E_{bg} for these materials by the Tauc method, a correction has to be made due to this value. The band gap for GCN was estimated in 2.70 eV, consistent with the literature, while the thermal treatment increased the Ebg of GCN(T) to 2.8 eV [26,36,83].

As for the metal doped materials (GCNM and GCN(T)M), a decrease in the E_{bg} is observed when compared to the reference material GCN and GCN(T), exception being made to the material with Pd (Figure 12 a and b), which is in accordance with literature[34]. For the Au composite, since there is no data regarding values of energy below 1.5 eV, the common method, without correction, was applied to estimate its band gap.

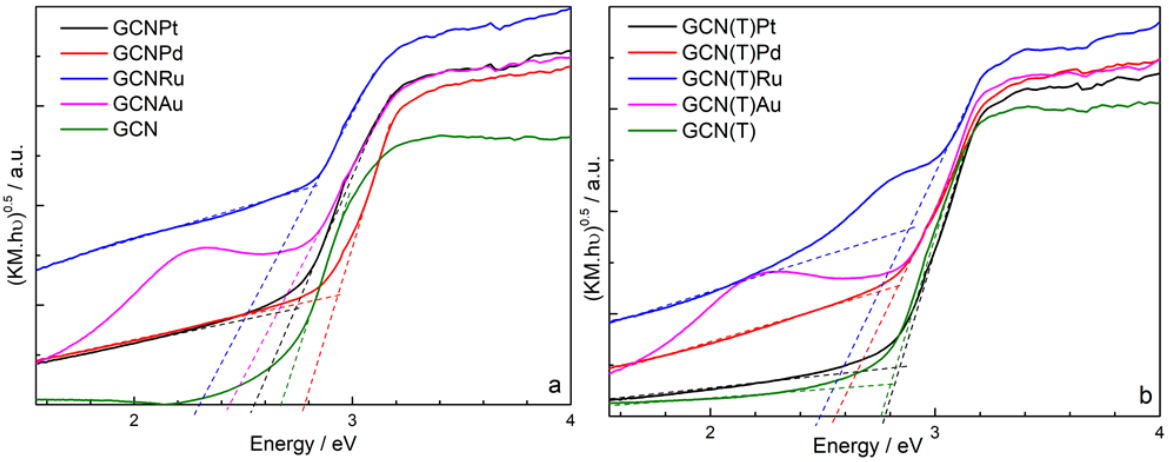

Figure 12 - Tauc plots for a) GCN and b) GCN(T) materials doped with metals (Pt, Pd, Ru, Au).

Table 3 - E_{bg} determined for undoped GCN, GCN(T) and doped with metals (Pt, Pd, Ru, Au).

Material	E_{bg} with correction / eV	E_{bg} without correction / eV
GCN	-	2.70
GCN(T)	-	2.80
GCNAu	-	2.42
GCNPd	2.79	2.95
GCNPt	2.58	2.78
GCNRu	2.25	2.81
GCN(T)Au	-	2.56
GCN(T)Pd	2.56	2.78
GCN(T)Pt	2.79	2.82
GCN(T)Ru	2.50	2.85

The molecular structure of these materials was further characterized by Fourier infrared (FTIR) spectroscopy. The FTIR spectra of GCN and GCN(T) (Figure 13), present the characteristic stretching vibrations around 3000-3400 cm^{-1} ascribed to -OH groups of surface adsorbed water molecules, and to the N-H stretches due to the free amino groups[37]. This band is more pronounced in the exfoliated material rather than in the bulk material probably due to the presence of higher amount of oxygen and terminal amino groups. Also, the characteristic peak of triazine rings[7] at 807 cm^{-1} is observed in both materials. This peak is more intense in the exfoliated material, indicating that there is a higher area available, corroborated by BET analysis. So, the material has more superficial groups that can vibrate, increasing the

transmittance of the spectra. The absence of band around 2200 cm^{-1}, characteristic of $N \equiv C$ in dicyandiamide (precursor) indicates that a complete polymerization occurred[34].

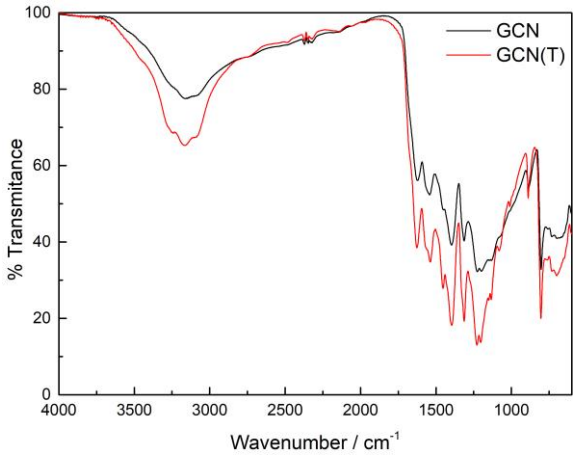

Figure 13 – FTIR spectra of GCN and GCN(T) materials.

The FTIR spectra of carbon nitride doped with metals was also studied and is presented in Figure 14. The characteristic peaks of carbon nitride are not changed when doping a metal phase to carbon nitride. Nevertheless, when Pd is doped in GCN, the characteristic peak of triazine does not have a significant intensity, comparing with the carbon phase or with the other metals. Also, the peaks of N-H, O-H and NH_2 stretching at 3200 cm^{-1} are much less intense in this material than in all others. This could be due to this material having aggregates or Pd covering carbon nitride.

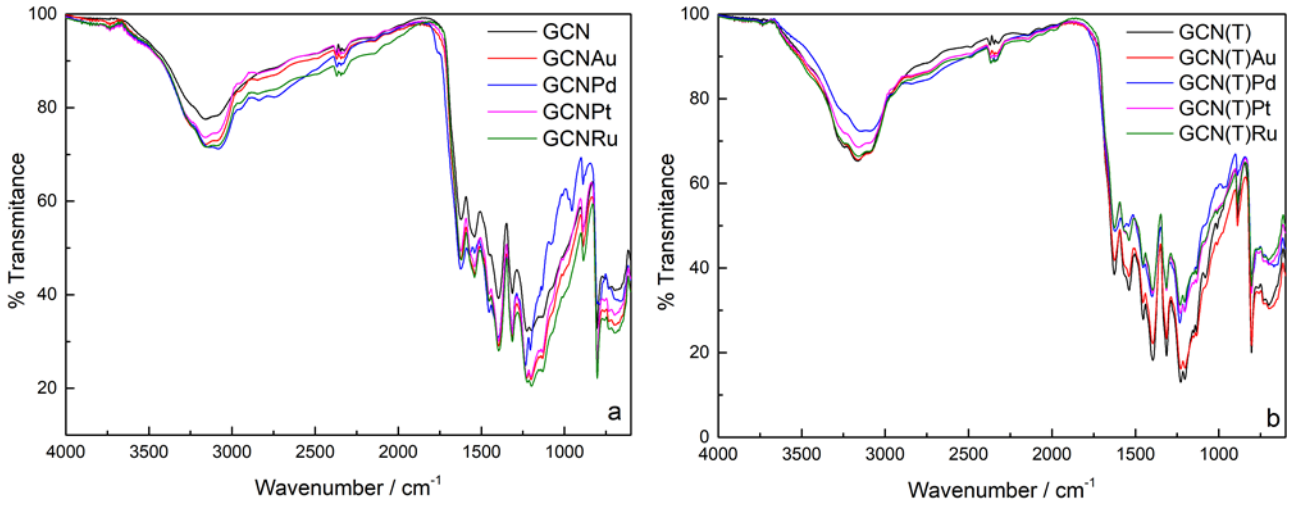

Figure 14 - FTIR spectra of a) GCN and b) GCN(T) materials doped with metals (Pt, Pd, Ru, Au).

To better understand the deposition of the metal particles in carbon nitride, TEM analysis was performed for GCN(T) doped with metals (Figure 15). It can be seen that Au, Pt and Ru

nanoparticles are better dispersed over the graphitic carbon nitride layers, as highlighted in the Figure 15.

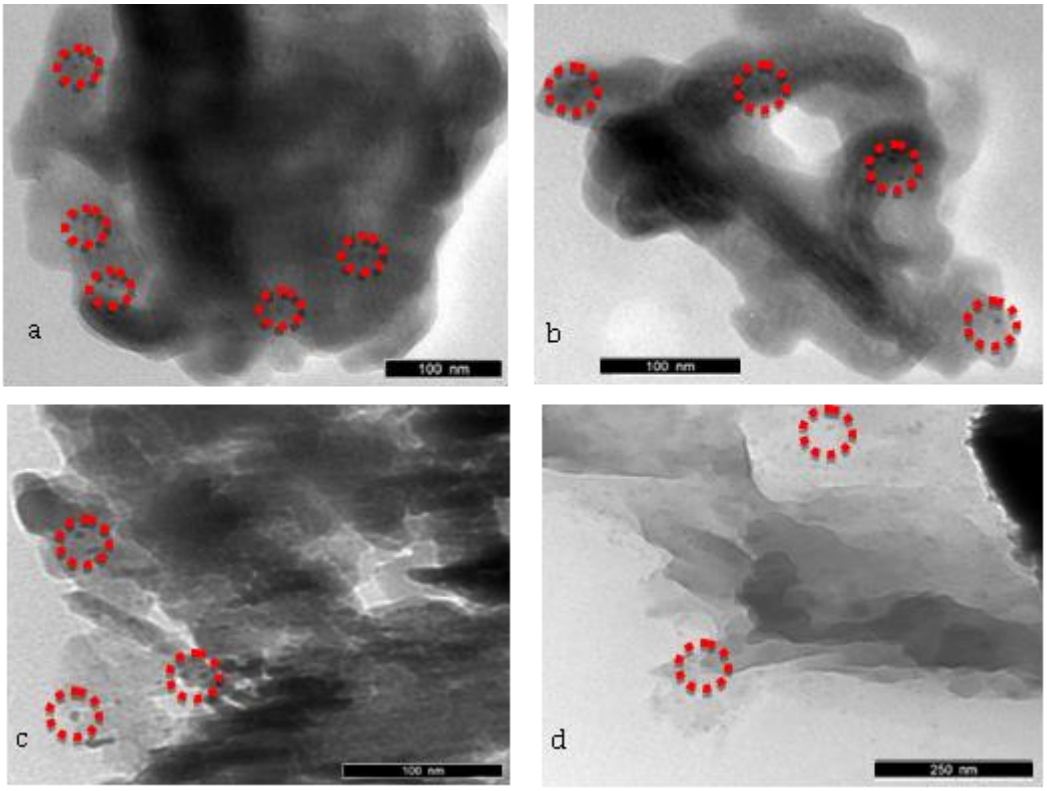

Figure 15 – TEM images of GCN(T) doped with metals a) Au, b) Pt, c) Ru, d) Pd.

Some important parameters of the deposition of metals were calculated from TEM, to obtain a homogeneous distribution and to diminish errors. These parameters are given in Table 4. Since none of the distributions is a gaussian distribution, instead of the standard deviation, the metal size range is presented. It is clear that Au has a relatively narrow and small metal range, with an average metal particle of 4.4 nm, indicating that its photocatalytic activity should be superior. Nevertheless, Ru has also a low average metal particle size, with a narrow metal size range, suggesting that the photocatalytic activity of this material should be high. Contrasting with Au, Pd has a big metal size range, with an average particle size of 8.7 nm, suggesting a low photocatalytic activity. The average metal particle size, mode and metal size range for these metals in carbon nitride is reported in the literature by Lima *et al*[34]. In general, the metal size range decreased to a narrower distribution when the support is the exfoliated carbon nitride, indicating a more homogeneous deposition of the metal particles.

Table 4 – Average particle size, mode and metal size range for metal doped GCN(T)M.

Metal	Average metal particle size / nm	Mode / nm	Metal size range / nm
Au	4.4	3-4	2-9
Pd	8.7	7-9	2-23
Pt	5.7	5-7	3-10
Ru	5.0	3-4	1-13

To better understand the surface properties of the materials, N_2 adsorption-desorption isotherms at 77 K was also performed to estimate the specific BET surface area (Table 5). While GCN has a surface area of 11 $m^{2}{\cdot}g^{-1}$, GCN(T) has a surface area of 143 $m^{2}{\cdot}g^{-1}$. The exfoliation of the carbon nitride increased substantially the surface area, indicating an effective separation of layers and higher availability of active sites. Doping a metal in the exfoliated material decreased greatly the surface area of the material except for Ru. This result could be explained by a good distribution and deposition of Ru nanoparticles in carbon nitride, not blocking pores. TEM images confirm a narrow distribution of Ru nanoparticles (Figure 15), indicating the non-formation of aggregates that could decrease the surface area of the material. This result is also confirmed by a decrease in the in PL intensity and more pronounced peaks in FTIR.

Table 5 - Specific surface area (S_{BET}) of undoped GCN and GCN(T) and of metal doped GCN(T).

Material	Surface area / $m^{2}{\cdot}g^{-1}$
GCN	11
GCN(T)	143
GCN(T)Au	55
GCN(T)Pt	57
GCN(T)Ru	140

N_2 adsorption-desorption analysis were also performed for the materials GCNPt and GCN(T)Pd. However, their results were not quantifiable. This is probably due to these materials having a low surface area, below the limit of detection of the equipment (5 $m^{2}{\cdot}g^{-1}$).

The morphology of the bare materials, GCN and GCN(T) was also analyzed by SEM (Figure 16). GCN presents typical graphitic, plate-like layered morphology consisting of solid agglomerates,

characteristic of a carbon nitride skeleton while the exfoliated material is much less dense than the bulk, indicating that an exfoliation in fact occurred, consistent with BET, PL and FTIR analysis[26].

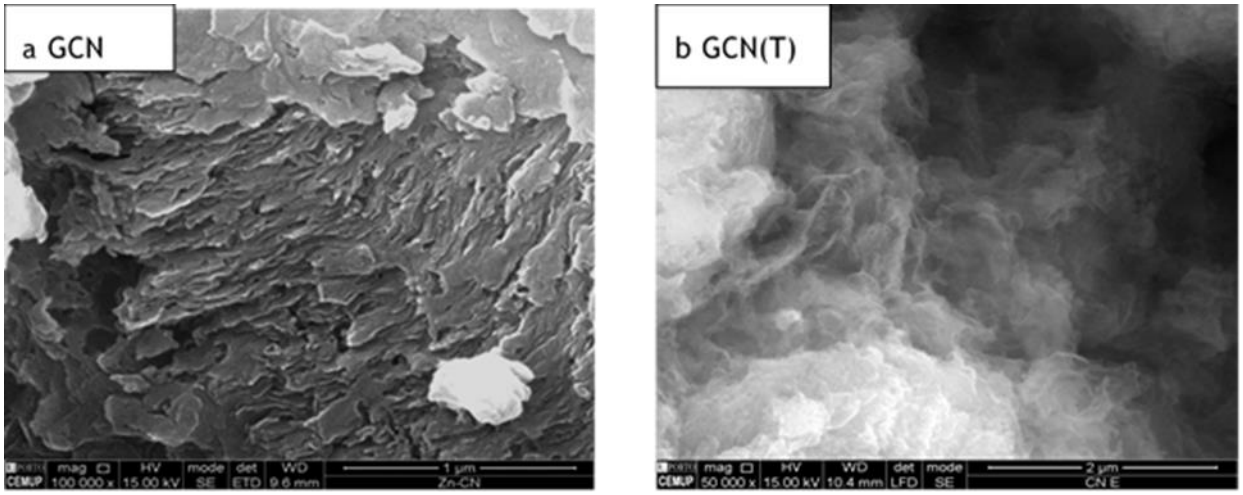

Figure 16 – SEM images of a) GCN and b) GCN(T) materials.

SEM images of GCNRu and GCN(T)Ru, as representative metal doped materials, are presented in Figure 17 a and b, respectively. In both figures it is possible to observe Ru well dispersed and distributed over the carbon nitride phase. However, when comparing with Figures 16, it is clear that the overall morphology of the carbon phase is not significantly changed.

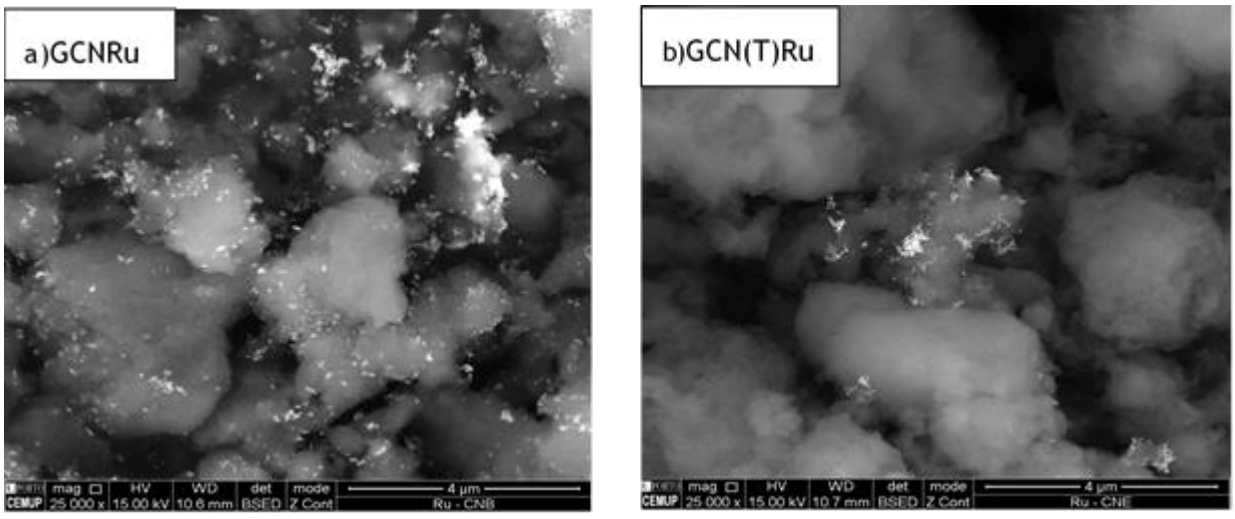

Figure 17 – SEM images of a) GCNRu and b) GCN(T)Ru materials.

4.2.2 MoS_2/graphitic carbon nitride composites

As given previously, the presence of noble metals induces significant changes in the structure of carbon nitride, enhancing the photoactivity of the material, as will be presented latter on (Chapter 4.3). However, these metals are expensive and with limited access, and it is becoming more urgent to find alternatives to replace them. Given that GCN(T) presents enhanced surface area, important to increase the photoactivity, this material was chosen to form composites (heterojunctions) with MoS_2 due to the electronic and optical compatibility of both materials[5].

Figure 18 shows the influence of the MoS_2 wt% on the PL spectra of GCN(T) as well as on the process used to prepare the composites (impregnation *vs* autoclave). As observed, there is an increase in the PL intensity when the composites are prepared by the impregnation method, regardless of the amount of MoS_2, comparing with pure GCN(T). However, when the autoclave method is used (GCN(T)M1.0A), a decrease of the emitted light is notorious, indicating that this composite could have a higher photocatalytic performance, due to a lower recombination of the charge-carriers. This result suggests that the physical mixture was insufficient to obtain a tight joint structure between both phases, contrary to observed in the autoclave method, in which an efficient heterojunction seems to be formed between carbon nitride and MoS_2[76]. In addition, a blue shift in the peak of maximum emission wavelength occurs when MoS_2 is added to GCN(T), for both preparation methods, but more pronounced in the autoclave method. This result could be explained by quantum size confinement.

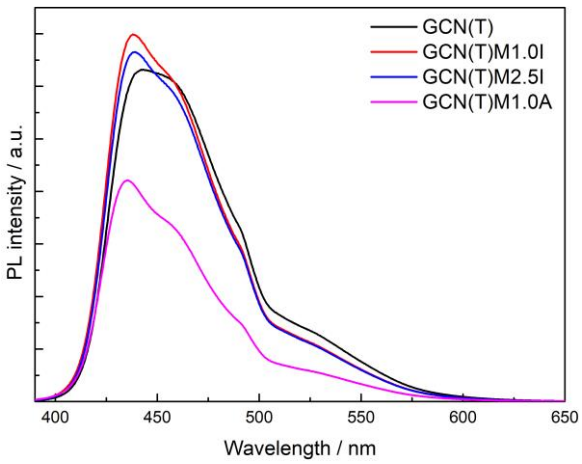

Figure 18 - PL spectra of bare GCN(T) and of GCN(T)MI and GCN(T)MA composites.

The absorption properties of the materials were studied by UV-Vis DR spectroscopy (Figure 19). When adding MoS_2 to GCN(T) using both methods, the absorption in the visible region is slightly enhanced although this increase is more significant in the material prepared in autoclave. Moreover, a significant increase in absorbance in the UV region (λ < 400 nm) is observed when

preparing the composite in the autoclave. This could result from better electrostatic interactions between MoS_2 and GCN(T), comparing with the impregnation method[28]. This result is in line with PL spectra (Figure 18).

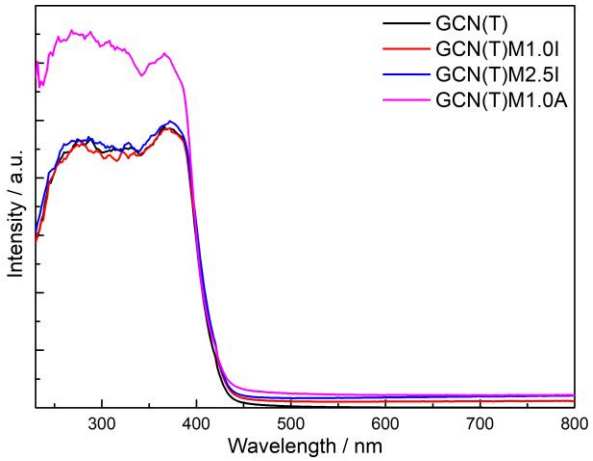

Figure 19 - UV-Vis DRS of bare GCN(T) and of GCN(T)MI and GCN(T)MA composites.

The Tauc plots were also performed for these materials and are presented in Figure 20 and the E_{bg} in Table 6. In particular, for these materials, the bang gap calculation, with or without the correction, is not significantly affected, due to the low values of Kubelka-Munk for low energy values. The composites prepared by impregnation present a slight increase in the E_{bg} while the composite prepared by autoclave shows a decrease, as compared to bare GCN(T).

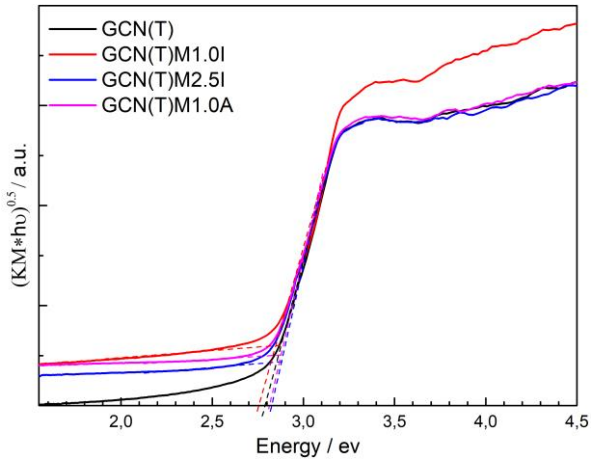

Figure 20 - Tauc plots of bare GCN(T) and of GCN(T)MI and GCN(T)MA composites.

Table 6 - E_{bg} with and without correction for bare GCN(T) and for GCN(T)MI and GCN(T)MA composites.

Material	E_{bg} with correction / eV	E_{bg} without correction / eV
GCN(T)	-	2.80
GCN(T)M1.0I	2.89	2.82
GCN(T)M2.5I	2.87	2.81
GCN(T)M1.0A	2.85	2.75

To better understand the surface properties of the prepared materials, N_2 adsportion-desorption analysis at 77 K was performed. For the composite with 2.5 wt% of MoS_2 prepared by the impregnation method a surface area of 123 $m^2 \cdot g^{-1}$ was obtained. Comparing with GCN(T) (Table 5), the specific surface area decreased by 14%, indicating that the structure of the material is slightly affected by the presence of MoS_2. However, other reports state that when a heterojunction is formed, the composite of carbon nitride and MoS_2 can have a higher surface area than bare carbon nitride, due to a larger area available[76]. This is consistent with our results, as seems that the impregnation method did not form an efficient heterojunction, as previously discussed.

The crystal structure of these materials was analyzed by X-ray diffraction (XRD). As shown in Figure 21, GCN(T) presents an intense diffract peak at 2θ ≈ 27.65°(002), characteristic of the graphitic carbon nitride layers stacking[26]. A less intense peak at 2θ ≈ 13° is observed, assigned to (100) in-plane structure of triazine polymeric units[26]. The MoS_2 material shows a characteristic peak at 2θ ≈ 14°, assigned to (002). This angle is lower than the one found in the reported literature, and could be explained to a higher spacing of the (002) plane [84]. This material has also a characteristic peak at 2θ ≈ 33° and 2θ ≈ 59°, assigned to (100) and (110) plane of hexagonal MoS_2[76,84]. Concerning the composites prepared by impregnation and in *in-situ*, both materials present the characteristic peaks of GCN(T), indicating that its structure is maintained. However, the composite prepared by in autoclave (*in-situ)* presents a small additional peak at 2θ ≈ 58° (110) characteristic of MoS_2, suggesting again the efficient formation of the heterojunction.

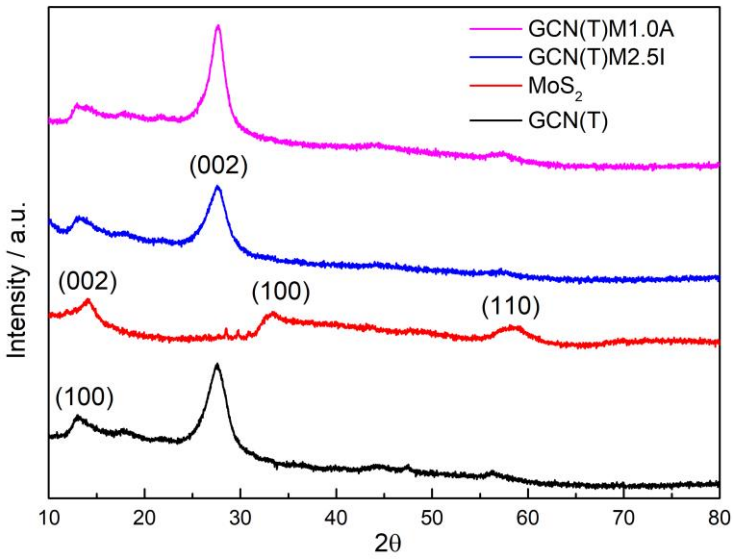

Figure 21 - XRD patterns of MoS_2, GCN(T) and of GCN(T)MI and GCN(T)MA composites.

The molecular structure of the materials was investigated by FTIR (Figure 22). The composites present similar vibrational spectra of GCN(T) (previously explained) although a slight shift of the triazine rings (807 cm^{-1}) occurs towards lower wavenumber when MoS_2 is present. This shift is more pronounced with the composite prepared by the *in-situ* method corroborating the PL, UV-Vis DRS and XRD data, indicating the formation of an efficient heterojunction between the two materials.

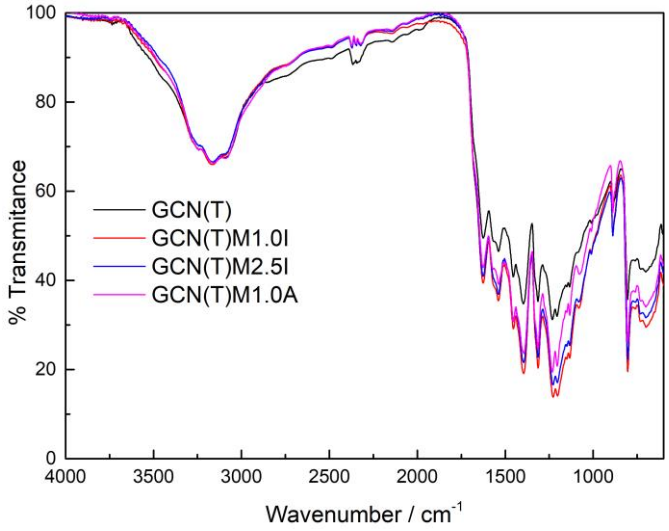

Figure 22 – FTIR spectra of bare GCN(T) and of GCN(T)MI and GCN(T)MA composites.

The morphology of MoS_2 and of the composites prepared by both methods is given in Figure 23. As shown in Figure 23a, MoS_2 presents a spherical petal cluster like-morphology, resembling to the “desert rose”. It is composed of thin layers, in the shape of open rose petals. This structure

is characteristic of bulk MoS_2, that can be destroyed after sonication[76]. The composite with 2.5 wt% MoS_2 prepared by impregnation method (Figure 23b) shows the presence of MoS_2 petals (brighter material) surrounded by carbon nitride (darker material). Yet, the composite prepared in the autoclave (Figure 23c) seems to present flake fragments of the petals (brighter material) which are also surrounded by exfoliated carbon nitride (darker material). It is possible that these fragments promote a better interaction between the two phases, therefore contributing for an efficient construction of MoS_2/GCN(T) heterojunction in opposite to the impregnation method.

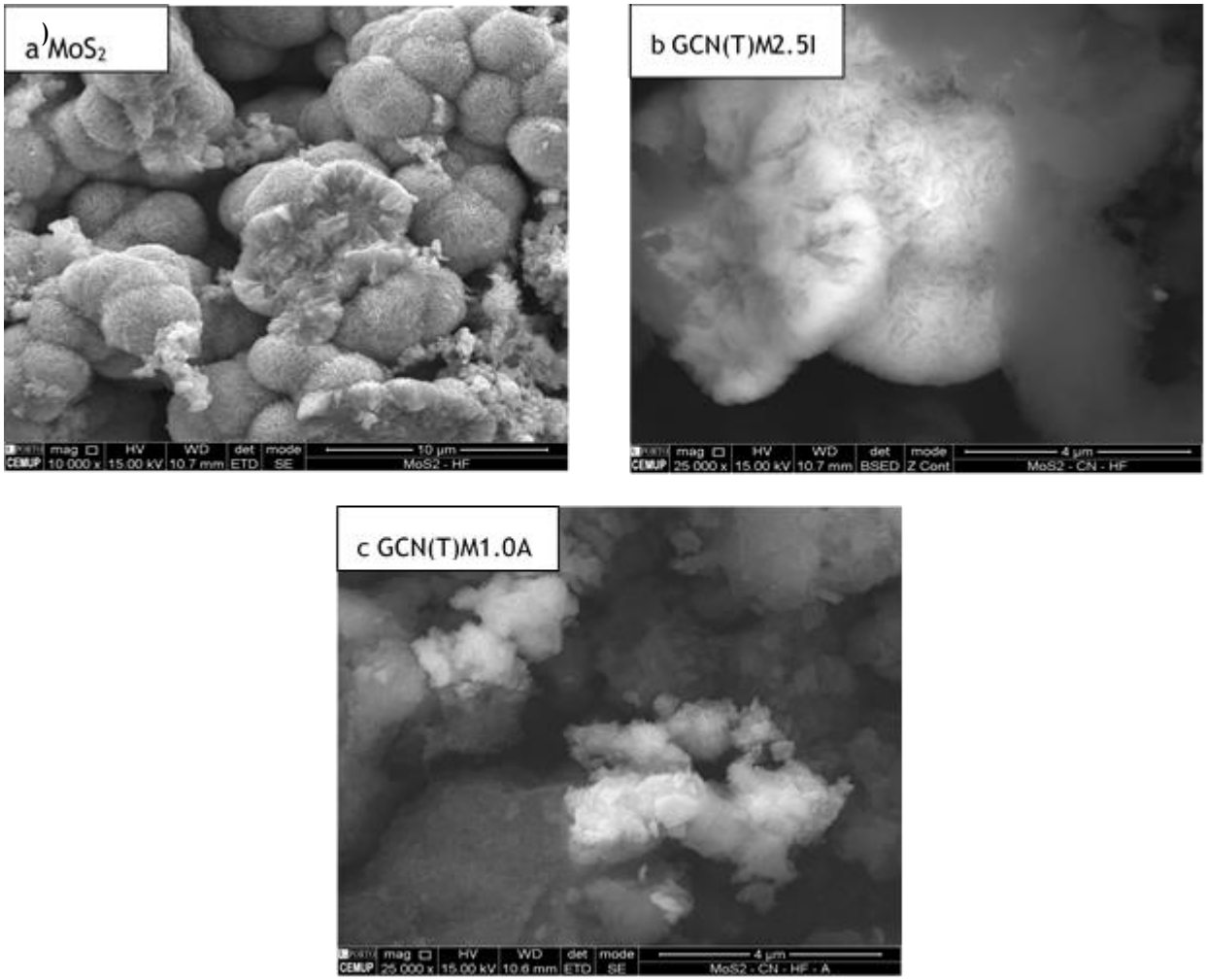

Figure 23 – SEM images of a) bare MoS_2 and of the composites b) GCN(T)M2.5I and GCN(T)M1.0A.

4.2.3 Non-metal doped carbon nitride

After the two approaches already discussed to modify the characteristics of graphitic carbon nitride (addition of metals and formation of heterojunctions with a co-catalyst), a third approach was performed, to obtain a greener way to overcome the limitations presented by

graphitic carbon nitride (high recombination of electron-hole and low absorption of light in the visible range). It is expected that these modifications will enhance the photoactivity of the prepared materials. As so, the process consisted in doping carbon nitride with a non-metal (phosphorus) and a combination of phosphorus-oxygen.

The PL emission spectra of the materials GCN, GCNP and GCNPO are given in Figure 24. As observed, the addition of P and PO greatly decreases the PL intensity comparing with GCN (Figure 24a), indicating a decrease in the recombination of the electron-hole pairs. This result is in line with other studies, which states that P-doped carbon nitride charge-carriers have a longer lifetime than in bare GCN, decreasing their recombination[38,39,85]. This PL results also suggests a superior photocatalytic activity of the non-metal doped materials comparing with bare GCN, since the recombination of the charge-carriers is a key step in photocatalysis. Moreover, the simultaneous doping of carbon nitride with P and PO further decreases the PL intensity, which indicates a lower recombination of the charge-carriers.

Since MoS_2 is a common co-catalyst for the production of solar fuels, towards the gradual replacement of Pt, composites of MoS_2 (1.0 wt%) with GCNP (GCNPM1.0A) and with GCNPO (GCNPOM1.0A) were prepared in autoclave. The PL spectra of these materials, displayed in Figure 24b, reveals that the addition of MoS_2 to the non-metal doped composites increases the PL intensity, indicating an increase in the recombination of the charge-carriers. However, the PL intensity is still much lower when comparing with GCN. Also, when adding MoS_2, a slight blue shift in the maximum wavelength of the peak occurs, consistent with the published literature[76].

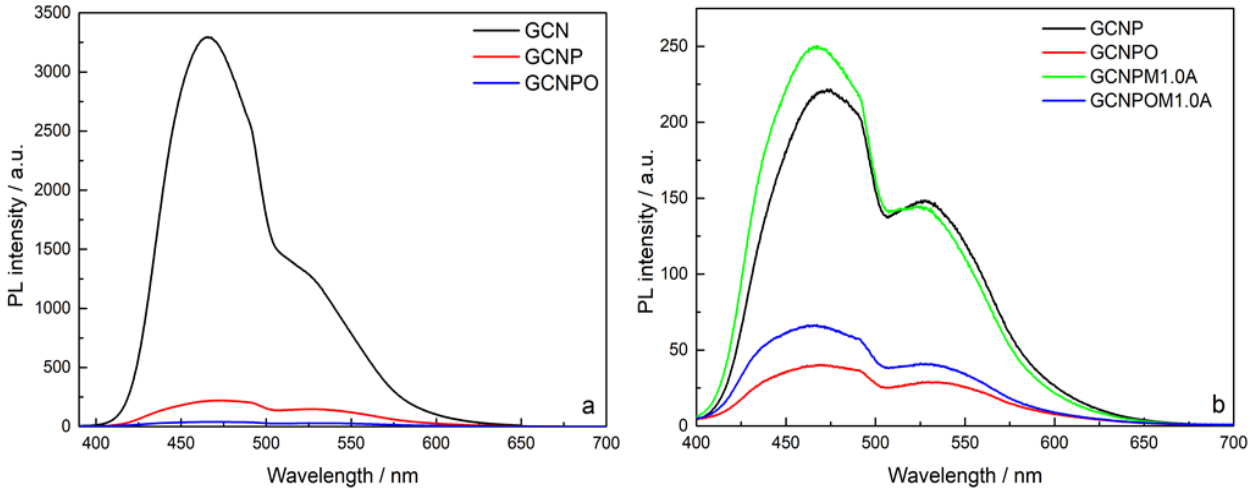

Figure 24 - PL spectra of a) bare GCN, GCNP and GCNPO and of b) GCNP and GCNPO and MoS_2 composites.

The effect of the non-metal doping in the absorption capacity of the materials was investigated by UV-Vis DRS (Figure 25). As shown, when GCN is doped with P, an increase in the absorbance

of the compounds is observed in the UV-Vis region of the spectra, with a with a broad absorption tail (Urbach tail) extending the optical absorption region from 450 nm to 800 nm[38,67,86]. Adding oxygen to this material further increases absorbance. These results are consistent with the colors of the materials, being darker (brown) than GCN (yellow). However, when adding MoS_2, a decrease in absorbance is noticed in both composites but more pronounced in the PO doped material, in agreement with PL results.

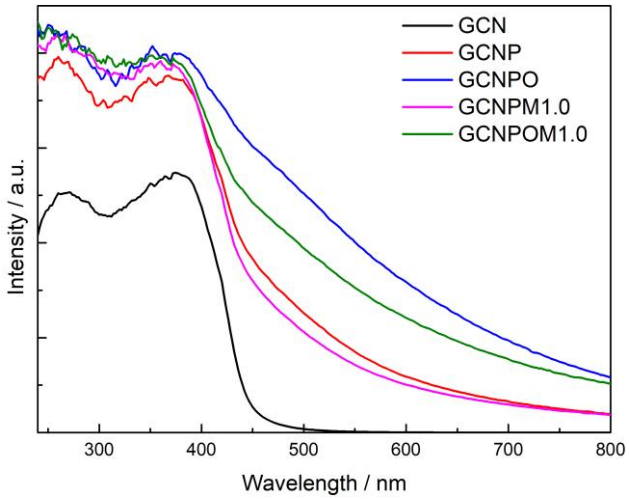

Figure 25 - UV-Vis DRS of non-metal doped GCN and of non-metal doped GCN/MoS_2 composites.

The Tauc plots for these materials were determined and presented in Figure 26, while the results are shown in Table 7. Due to the lack of results for low energy values, and these values being relatively small, no correction was performed to the band gap energy. For the GCNPO material no band gap energy was calculated due to these materials having midgaps states, creating a Urbach tail, that extended the absorption region from 450 nm to 800 nm, not allowing a correct band gap energy. As shown in Table 7, the addition of MoS_2 to GCNP does not substantially changes the band gap energy. This result is probably due to a low wt% of MoS_2 in carbon nitride. However, doping oxygen in addition to P decreases considerably the E_{bg} of the material to 1.75 eV.

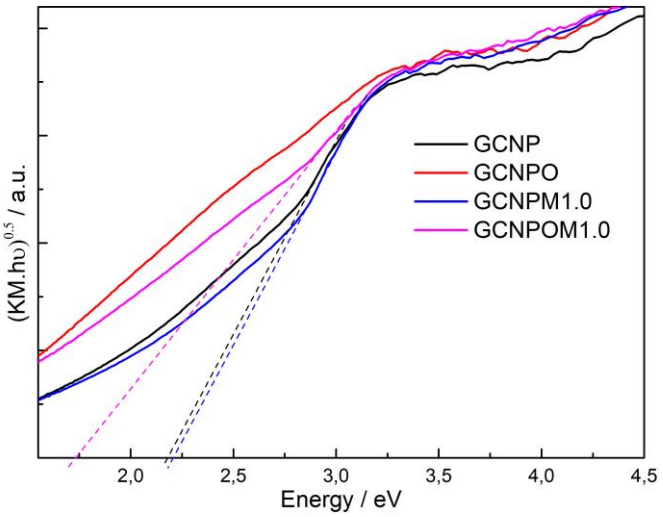

Figure 26 - Tauc plots for non-metal doped GCN and for non-metal doped GCN/MoS_2 composites.

Table 7 – E_{bg} with and without correction for GCNP, GCMPM1.0A and GCNPOM1.0A materials.

Material	E_{bg} with correction / eV	E_{bg} without correction / eV
GCNP	-	2.21
GCNPM1.0A	-	2.23
GCNPOM1.0A	-	1.75

N_2 adsorption-desorption analysis was also performed for the non-metal doped materials, however, their results were not quantifiable and should therefore be repeated to assess its reproducibility.

The materials were further characterized by FTIR (Figure 27). No significant changes occur in the vibrational spectra of the different doped materials, comparing with GCN, except for a decrease in the intensity of the characteristic peak around 3200 cm^{-1}, corresponding to the amino groups and hydroxyl groups. This might be related with less N-H bonds, due to nitrogen atoms in the structure of carbon nitride being replaced by phosphorus and oxygen.

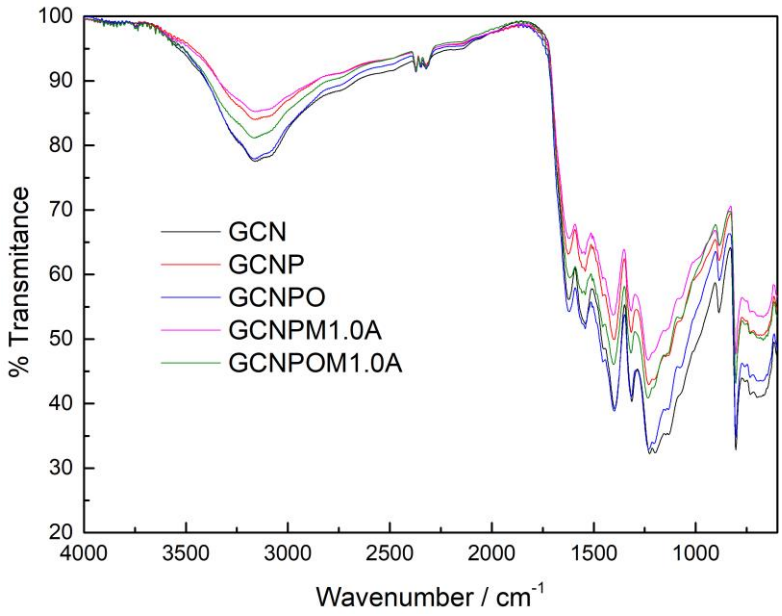

Figure 27 – FTIR spectra for non-metal doped GCN and for non-metal doped GCN/MoS_2 composites.

The SEM image for GCNP is presented in Figure 28. The morphology of the material resembles the one of bare GCN (Figure 16a), with layers but also with some porous particles, indicating that the doping of phosphorus changes the overall morphology of the material. It is known that the presence of porous in the structure of the materials can enhance light harvesting because of the multiple reflections within an interconnected open-framework, as well as influence the transfer pathway of the charge-carriers, thus increasing the photocatalytic activity of the material[37].

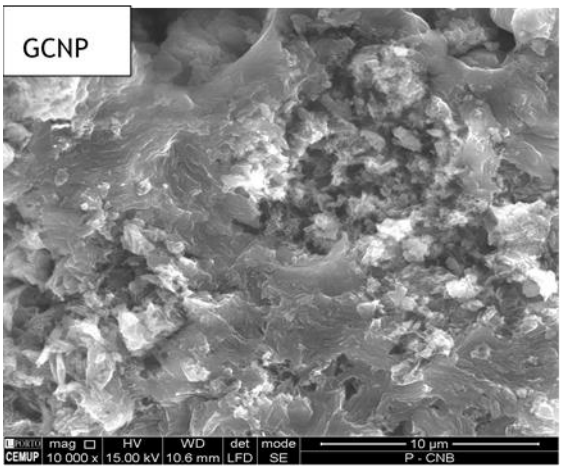

Figure 28 – SEM image of GCNP material.

4.2.4 MoS_2/reduced graphene oxide

The electronic and optical properties of the MoS_2/reduced graphene oxide (abbreviated as GOM) were characterized by PL and UV-Vis DR spectra (Figures 29 and 30). The PL spectra (Figure 29) of MoS_2 shows emission in the UV-Vis region, with maximum wavelength around 450 nm. The PL spectra of the composites is similar to the one of MoS_2, however, the amount of MoS_2 loaded in graphene generates changes in PL intensity. The composite with 10 wt% of MoS_2 presents the lowest PL intensity while the loading of 20 wt% lead to a higher PL intensity, suggesting an overload of MoS_2. Therefore, the composite with 10 wt% of MoS_2 in reduced graphene oxide could be, eventually, the optimum amount due to the lower intensity of the emitted light, indicative of lower electron-hole recombination.

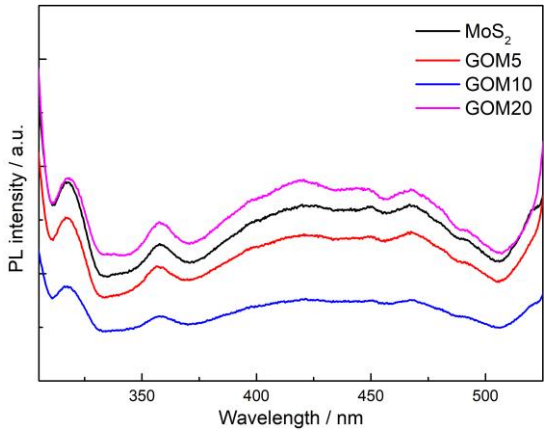

Figure 29 – PL spectra of MoS_2 and of GOM materials.

The UV-Vis absorption capacity of these materials is presented in Figure 30. As shown, MoS_2 presents absorption in entire UV-Vis region of the spectra. Adding MoS_2 to graphene oxide increases the absorption of light of the material when comparing with MoS_2, consistent with the literature[49]. However, this absorption is not linear with the increase of MoS_2. The composite with 10 wt% of MoS_2 has the higher absorption of light, contrasting with the composite with 20 wt% that has an intermediary response between the 5 wt% and 10 wt% composite. This result for GOM10 combined with the result of PL indicates that this material could have a superior photocatalytic activity, due to a higher absorption of light in the visible range of the spectra and a decrease in the PL intensity, which implies a lower recombination of the charge-carriers.

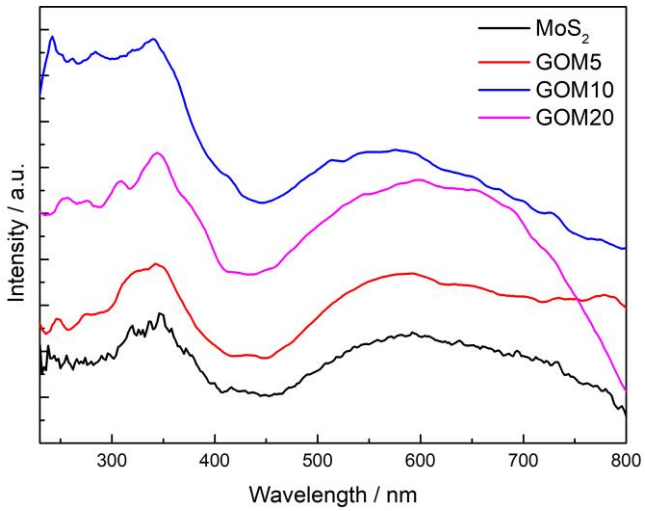

Figure 30 – UV-Vis DR spectra of MoS_2 and GOM materials.

These materials were characterized by FTIR spectra (Figure 31). The addition of MoS_2 to reduced graphene oxide decreases the intensity of the characteristic peaks of MoS_2. However, in all composites, its characteristic peaks are visible, but with different intensities. The behavior in FTIR spectra is consistent with the UV-Vis DRS and PL analysis.

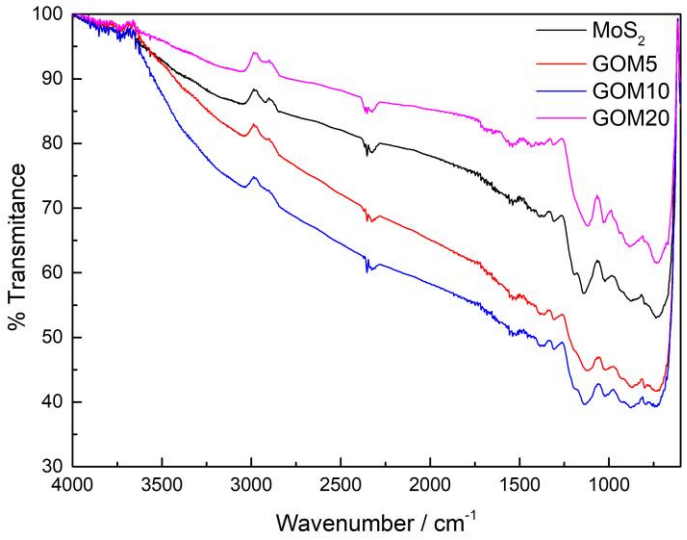

Figure 31 – FTIR spectra of MoS_2 and of GOM materials.

The morphology of MoS_2 and the composite GOM20 was investigated by SEM. Figure 32 shows the composite of 20 wt% MoS_2 with rGO. This material has a structure of platelets with rGO wrapping the material. The morphology of the material appears to have also a veil (center of image), also with rGO wrapping the material.

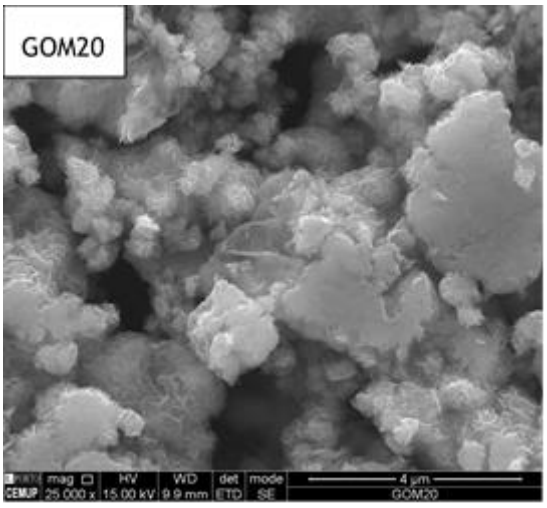

Figure 32 – SEM image for the composite GOM20.

4.3 Solar fuels production

4.3.1 Photocatalytic hydrogen production

The activity of the as prepared materials was tested towards the photocatalytic H_2 production and compared with the bare materials (GCN and GCN(T)). Normally, the photocatalytic evolution of H_2 from water requires the use of three main components: a catalyst capable of absorbing light, a sacrificial electron donor to regenerate the catalyst and a co-catalyst to perform the reduction of water. All the reactions were performed with 0.3 $g \cdot L^{-1}$ of catalyst, 15% vol. of EDTA (electron donor) and 1 wt% of co-catalyst (Pt nanoparticles or MoS_2). LEDs, emitting at maximum wavelength of 423 nm were employed as the light source. Blank tests of no catalysts and no light were performed to confirm the effective production of H_2. However, longer reactions should be performed in future work to better understand the stability of the catalysts.

It is important to state that the photocatalytic test employing the materials GCN, GCN(T), GCNP, GCNPO required the particular addition of Pt nanoparticles (1 wt%) as co-catalyst to boost the hydrogen production.

The results concerning the photocatalytic production of H_2 for all the materials is displayed in Figures 33-35. From this data it is possible to observe that the metal doped photocatalysts have the highest production of hydrogen among all tested materials.

The photocatalytic H_2 production for carbon nitride doped with metals is presented in Figure 33. A comparison between the amount of H_2 produced between bare GCN (Figure 33a) and bare GCN(T) (Figure 33b) reveals a more efficient production by GCN(T), which can mainly be

ascribed by the higher surface of GCN(T) (143 *vs* 11 $m^{2}\cdot g^{-1}$). All the metal doped materials present higher production of H_2 than bare ones, regardless of using GCN or GCN(T). However, best performances are obtained when the base catalyst is GCN(T) (Figure 33b), with the exception of Pd, which can be related with the higher surface area. In particular, Pt is the best metal doped in GCN while Ru is the best metal doped in GCN(T), with a hydrogen production of 16904 $\mu mol\cdot g^{-1}\cdot h^{-1}$. This result is higher than the reported literature, presented in the context of the art chapter, and might be explained by the lowest PL intensity (indicating a lower recombination of the electron-hole), the highest absorption of light in the visible region of the spectra and the lowest average particle size. On the other side, the GCN(T)Pt has also a H_2 production superior comparing with the reported literature, probably due to the good compromise between the average particle size, the PL intensity and to the absorption of light.

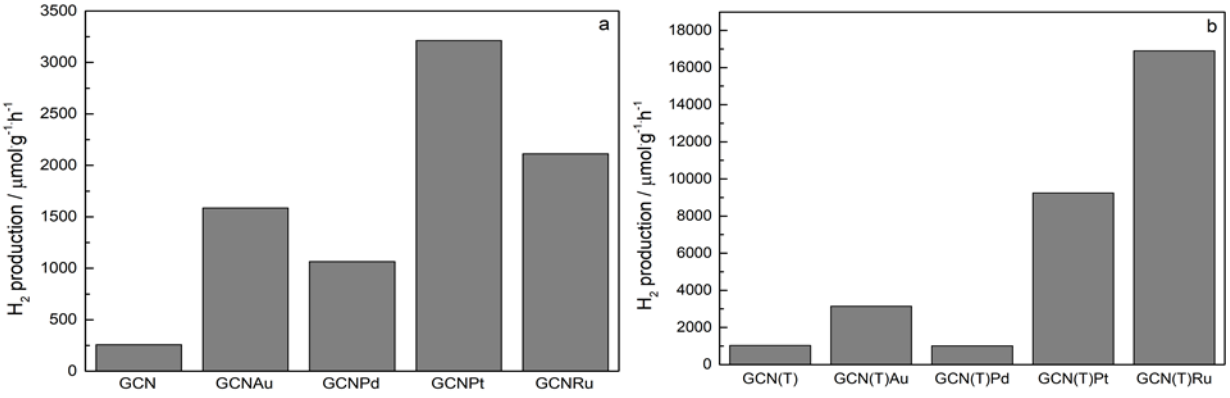

Figure 33 – Photocatalytic H_2 evolution rates of a) GCN and b) GCN(T) materials doped with metals (Pt, Pd, Ru, Au) after 2h of visible irradiation.

The photocatalytic results concerning H_2 production by non-metal doped bulk carbon nitride are shown in Figure 34. In this case, the photocatalytic activity of GCNP and GCNPO was compared with GCN activity when using Pt nanoparticles as co-catalyst. Under these conditions, GCNP enhanced the H_2 production by a factor of 1.4 while the addition of PO has an opposite effect on the activity. The higher activity of GCNP can be related with the higher absorbance at the irradiation wavelength (Figure 25) and lower electron-hole recombination (Figure 24). Other studies related with non-metal doping of graphitic carbon nitride, including P and C, report an increase in the H_2 production due to a synergistic effect between the C/P particles and the graphitic carbon nitride[37,86].

The lower H_2 production of GCNPO can be related with the presence of midgaps and the position of the CB and VB. It is possible that these are not appropriate to carry out water reduction. Further studies, mainly XPS analysis and electrochemical analysis have to be performed to

obtain insights of these values. When MoS_2 replaced Pt nanoparticles as co-catalyst, both GCNPM1.0A and GCNPOM1.0A composites were able to produce H_2, demonstrating the alternative use of greener materials as MoS_2 as co-catalysts. Once again, GCNPM1.0A produced a higher amount of H_2 rather than GCNPOM1.0A, possibly due to the same reasons mention above. GCNPO showed practically the same activity of the composite GCNPOM1.0A, indicating that for this material, the co-catalyst MoS_2 has the same influence as the solution of Pt nanoparticles.

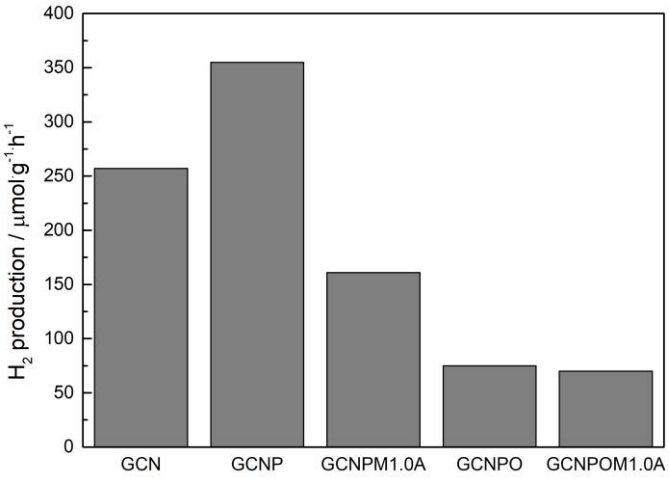

Figure 34 – Photocatalytic H_2 evolution rates for non-metal doped carbon nitride and for non-metal doped GCN/MoS_2 composites after 2h of visible irradiation.

The photocatalytic activity of the composites MoS_2/GCN(T) and GOM20 were also carried out (Figure 35). From the results it is possible to observe that the H_2 production for the composites GCN(T)M1.0I, GCN(T)M2.5I and GCN(T)M1.0A is dependent both on the amount of MoS_2 loaded and synthesis procedure used to construct the composites. Concerning the composites prepared by impregnation, loading with 2.5 wt% of MoS_2 generates a higher photoactivity (1.6 times) than the composite containing 1.0 wt%, indicating that MoS_2 serves efficiently as a co-catalyst. Further studies should be done to find the optimal amount of MoS_2. When the *in-situ* method (autoclave) is applied to prepare the composite with 1.0 wt% of MoS_2 (GCN(T)M1.0A), the hydrogen production of this material in 2.8 times enhanced comparing with the same amount of MoS_2 in the catalyst prepared by the impregnation method (GCN(T)M1.0I). The catalyst prepared in the autoclave has a higher absorption of light and decreased PL intensity. As corroborated by the characterization (PL and UV-Vis DRS), this performance results from the creation of a more efficient heterojunction between two constituents of the material, which hindered the recombination of electron-hole, inherent to the preparation method[76]. The impregnation method, as a physical mixture of the materials, does not induces great differences in the properties of the material. Nevertheless, further tests should be carried out and more

catalysts prepared, with different amounts of MoS_2, to determinate the optimum amount of MoS_2 in GCN(T), using the autoclave to prepare the heterojunctions. Concerning the composite of graphene oxide with 20 wt% of MoS_2 (GOM20), a low amount of hydrogen was produced after 2h of reaction (Figure 35). Although this material has a high absorption of light in the visible range of the spectra, its PL spectra indicates that there is a high recombination of charge-carriers, thus, decreasing the number of electrons available to produce hydrogen. The other GOM composites still have to be tested for the hydrogen production, although it is expectable that GOM10 will give better activity, taking in consideration all the properties discussed in previous chapter.

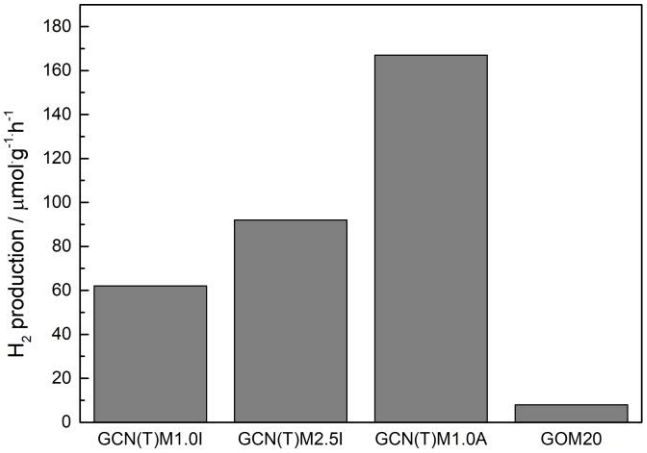

Figure 35 - Photocatalytic H_2 evolution rates for MoS_2/GCN(T) and GOM20 composites after 2h of visible irradiation.

4.3.2 CO_2 photoreduction into fuels

The screening of these materials for the CO_2 reduction into fuels also started to being tested. In the gas phase it is expected to determinate CO and, eventually, CH_4. In the liquid phase it is expected to determinate MeOH and EtOH and, eventually, formic acid. However, the analytical methods in the gas chromatographer need to be optimized before further photocatalytic studies are carried out, to perform gas and liquid analyses simultaneously.

5 Conclusions

The photocatalytic production of solar fuels, in particular, the production of hydrogen, is one promising route to outcome an upcoming energy crisis. Nevertheless, it is clear that these technologies are not yet capable of suppressing the energy demands of human life, mainly due to the utilized materials not being selective and capable of producing a considerable amount of the desired fuel.

2D carbon-based materials were synthesized and characterized by several different important techniques which contribute to explain the photocatalytic activity. Graphitic carbon nitride and reduced graphene oxide have been studied in the past years and their application is well known. However, their characteristics still limits their activity, in particular in the solar fuels department.

MoS_2 has proven to be an effective co-catalyst, both in carbon nitride and in reduced graphene oxide, able to replace noble-metal doping in the future. Nevertheless, further investigation on the synthesis procedure should be performed, to optimize the amount of this co-catalyst and the synthesis method, to take advantage of all the potential this material has. Also, the exfoliation of MoS_2 should be performed, to create nanosheets, with better electronic properties.

The modifications performed to graphitic carbon nitride had a significant effect in the final material, with the thermal exfoliation and the doping being effective for the photocatalytic production of hydrogen. Also, these materials are expected to have potential in other photocatalytic processes, such as CO_2 photoreduction, due to their unique and advantage properties.

Overall, it was possible to observe that the structure of the materials has a great influence on the photocatalytic activity, and that the approaches made in this work are promising to overcome the limitations presented by the nowadays utilized materials.

6 Assessment of the work done

6.1 Objectives Achieved

The primary objective of this Dissertation is the development of photocatalysts, mainly 2D materials,that can be applied to solar fuels production. In that respect, more than 20 different materials, organized in three big groups, were prepared: materials based on graphitic carbon nitride, molybdenum disulfide and reduced graphene oxide.

They were extensively characterized by UV-Vis diffuse reflectance, infra-red and photoluminescence spectroscopies, scanning and transmission electron microscopies, X-ray diffraction and N_2 adsorption-desorption isotherms.

Finally, the activity of the materials was tested towards the photocatalytic production of hydrogen through water splitting using Light Emitting Diodes (LEDs) as a visible light source.

6.2 Other Work Carried Out

During the project, it was necessary to relocate the working station for setting up the reaction and analysis equipment. This involved the dislocation of the analysis equipment and installation on the new location. Also, the chromatographic methods concerning CO_2 photoreduction needed to be reformulated, which was partially done, being still a task under development.

6.3 Limitations and Future Work

The practical aspects for production of solar fuels need to be correctly addressed. Currently is in course the development of a dedicated solar simulator to test the developed materials. Several issues related with the product analysis concerning the photocatalytic reduction of CO_2 limited the progression in this direction. To overcome these a full makeover of the existing GC is now in progress.

Finally, the produced photocatalytic materials need to integrated in conceptual prototypes that will render the process, even more attractive that it is already.

6.4 Final Assessment

The development of selective and efficient photocatalysts for solar fuels is urgent, having in mind that an energy crisis could be in the near future. The applied techniques gave another perspective regarding the materials, with the different doping and tuning performed to the materials, bringing a wider insight to the group, within this subject. This dissertation, being the last check-point of my course, has without a doubt, contributed to my future.

7 References

1. Liu, L., Ke, C. C., Ma, T. Y., Zhu, Y. P. When carbon meets CO_2: Functional carbon nanostructures for CO_2 utilization. *Journal of Nanoscience and Nanotechnology*. **2019,** *19*, 3148-3161.

2. Maginn, E. J. What to do with CO_2. *Journal of Physical Chemistry Letters*. **2010,** *1*, 3478-3479.

3. Tahir, M., Amin, N. S. Recycling of carbon dioxide to renewable fuels by photocatalysis: Prospects and challenges. *Renewable and Sustainable Energy Reviews*. **2013,** *25*, 560-579.

4. Chen, Y., Jia, G., Hu, Y., Fan, G., Tsang, Y. H., Li, Z., Zou, Z. Two-dimensional nanomaterials for photocatalytic CO_2 reduction to solar fuels. *Sustainable Energy & Fuels*. **2017,** *1*, 1875-1898.

5. Hou, Y., Laursen, A. B., Zhang, J., Zhang, G., Zhu, Y., Wang, X., Dahl, S., Chorkendorff, I. Layered nanojunctions for hydrogen-evolution catalysis. *Angewandte Chemie Int Ed*. **2013,** *52*, 3621-3625.

6. Ye, S., Wang, R., Wu, M.-Z., Yuan, Y.-P. A review on g-C_3N_4 for photocatalytic water splitting and CO_2 reduction. *Applied Surface Science*. **2015,** *358*, 15-27.

7. Yan, J., Chen, Z., Ji, H., Liu, Z., Wang, X., Xu, Y., She, X., Huang, L., Xu, L., Xu, H., Li, H. Construction of a 2D graphene-like MoS_2/C_3N_4 heterojunction with enhanced visible-light photocatalytic activity and photoelectrochemical activity. *Chemistry - A European Journal*. **2016,** *22*, 4764 –4773.

8. Mills, A., Le Hunte, S. An overview of semiconductor photocatalysis. *Journal of Photochemistry and Photobiology A: Chemistry*. **1997,** *108*, 1-35.

9. Wang, W.-N., Soulis, J., Yang, Y. J., Biswas, P. Comparison of CO_2 photoreduction systems: A review. *Aerosol and Air Quality Research*. **2014,** *14*, 533-549.

10. Khan, A. A., Tahir, M. Recent advancements in engineering approach towards design of photo-reactors for selective photocatalytic CO_2 reduction to renewable fuels. *Journal of CO_2 Utilization*. **2019,** *29*, 205-239.

11. Lingampalli, S. R., Ayyub, M. M., Rao, C. N. R. Recent progress in the photocatalytic reduction of carbon dioxide. *ACS Omega*. **2017,** *2*, 2740-2748.

12. Mao, J., Li, K., Peng, T. Recent advances in the photocatalytic CO_2 reduction over semiconductors. *Catalysis Science & Technology*. **2013,** *3*, 2481-2498.

13. Tauc, J., Grigorovici, R., Vancu, A. Optical properties and electronic structure of amorphous germanium. *Physica status solidi (b)*. **1966,** *15*, 627-637.

14. Makuła, P., Pacia, M., Macyk, W. How to correctly determine the band gap energy of modified semiconductor photocatalysts based on UV–Vis spectra. *The Journal of Physical Chemistry Letters*. **2018,** *9*, 6814-6817.

15. Hsu, H.-C., Shown, I., Wei, H.-Y., Chang, Y.-C., Du, H.-Y., Lin, Y.-G., Tseng, C.-A., Wang, C.-H., Chen, L.-C., Lin, Y.-C., Chen, K.-H. Graphene oxide as a promising photocatalyst for CO_2 to methanol conversion. *Nanoscale*. **2013,** *5*, 262-268.

16. Sun, H., Wang, S. Research advances in the synthesis of nanocarbon-based photocatalysts and their applications for photocatalytic conversion of carbon dioxide to hydrocarbon fuels. *Energy & Fuels*. **2014,** *28*, 22-36.

17. Crake, A., Christoforidis, K. C., Godin, R., Moss, B., Kafizas, A., Zafeiratos, S., Durrant, J. R., Petit, C. Titanium dioxide/carbon nitride nanosheet nanocomposites for gas phase CO_2 photoreduction under UV-visible irradiation. *Applied Catalysis B: Environmental*. **2019,** *242*, 369-378.

18. Low, J., Cheng, B., Yu, J., Jaroniec, M. Carbon-based two-dimensional layered materials for photocatalytic CO_2 reduction to solar fuels. *Energy Storage Materials*. **2016,** *3*, 24-35.

19. Sun, Z., Wang, H., Wu, Z., Wang, L. g-C_3N_4 based composite photocatalysts for photocatalytic CO_2 reduction. *Catalysis Today*. **2018,** *300*, 160-172.

20. Jin, B., Yao, G., Jin, F., Hu, Y. H. Photocatalytic conversion of CO_2 over C_3N_4-based catalysts. *Catalysis Today*. **2018,** *316*, 149-154.

21. Mao, J., Peng, T., Zhang, X., Li, K., Ye, L., Zan, L. Effect of graphitic carbon nitride microstructures on the activity and selectivity of photocatalytic CO_2 reduction under visible light. *Catalysis Science and Technology*. **2013,** *3*, 1253-1260.

22. Bhosale, R., Jain, S., Vinod, C. P., Kumar, S., Ogale, S. Direct Z-Scheme g-C_3N_4/$FeWO_4$ nanocomposite for enhanced and selective photocatalytic CO_2 reduction under visible light. *ACS Applied Materials and Interfaces*. **2019,** *11*, 6174-6183.

23. Pastrana-Martínez, L. M., Morales-Torres, S., Likodimos, V., Figueiredo, J. L., Faria, J. L., Falaras, P., Silva, A. M. T. Advanced nanostructured photocatalysts based on reduced graphene oxide–TiO_2 composites for degradation of diphenhydramine pharmaceutical and methyl orange dye. *Applied Catalysis B: Environmental*. **2012,** *123-124*, 241-256.

24. He, Y., Wang, Y., Zhang, L., Teng, B., Fan, M. High-efficiency conversion of CO_2 to fuel over ZnO/g-C_3N_4 photocatalyst. *Applied Catalysis B: Environmental*. **2015,** *168-169*, 1-8.

25. Yu, J., Jin, J., Cheng, B., Jaroniec, M. A noble metal-free reduced graphene oxide-CdS nanorod composite for the enhanced visible-light photocatalytic reduction of CO_2 to solar fuel. *Journal of Materials Chemistry A*. **2014,** *2*, 3407-3416.

26. Lima, M. J., Silva, A. M. T., Silva, C. G., Faria, J. L. Graphitic carbon nitride modified by thermal, chemical and mechanical processes as metal-free photocatalyst for the selective synthesis of benzaldehyde from benzyl alcohol. *Journal of Catalysis*. **2017,** *353*, 44-53.

27. Tang, J. Y., Yang, D., Zhou, W. G., Guo, R. T., Pan, W. G., Huang, C. Y. Noble-metal-free molybdenum phosphide co-catalyst loaded graphitic carbon nitride for efficient photocatalysis under simulated irradiation. *Journal of Catalysis*. **2019,** *370*, 79-87.

28. Da Silva, E. S., Moura, N. M. M., Neves, M. G. P. M. S., Coutinho, A., Prieto, M., Silva, C. G., Faria, J. L. Novel hybrids of graphitic carbon nitride sensitized with free-base meso - tetrakis(carboxyphenyl) porphyrins for efficient visible light photocatalytic hydrogen production. *Applied Catalysis B: Environmental*. **2018,** *221*, 56-69.

29. Shi, G., Yang, L., Liu, Z., Chen, X., Zhou, J., Yu, Y. Photocatalytic reduction of CO_2 to CO over copper decorated g-C_3N_4 nanosheets with enhanced yield and selectivity. *Applied Surface Science*. **2018,** *427*, 1165-1173.

30. Kong, L., Yan, J., Liu, S. F. Carbonyl linked carbon nitride loading few layered MoS_2 for boosting photocatalytic hydrogen generation. *ACS Sustainable Chemistry and Engineering*. **2019,** *7*, 1389-1398.

31. Thanh Truc, N. T., Giang Bach, L., Thi Hanh, N., Pham, T. D., Thi Phuong Le Chi, N., Tran, D. T., Nguyen, M. V., Nguyen, V. N. The superior photocatalytic activity of Nb doped TiO_2 /g-C_3N_4 direct Z-scheme system for efficient conversion of CO_2 into valuable fuels. *Journal of Colloid and Interface Science*. **2019,** *540*, 1-8.

32. Xu, H., Yan, J., She, X., Xu, L., Xia, J., Xu, Y., Song, Y., Huang, L., Li, H. Graphene-analogue carbon nitride: novel exfoliation synthesis and its application in photocatalysis and photoelectrochemical selective detection of trace amount of Cu^{2+}. *Nanoscale*. **2014,** *6*, 1406-1415.

33. Zhao, H., Yu, H., Quan, X., Chen, S., Zhang, Y., Zhao, H., Wang, H. Fabrication of atomic single layer graphitic-C_3N_4 and its high performance of photocatalytic disinfection under visible light irradiation. *Applied Catalysis B: Environmental*. **2014,** *152-153*, 46-50.

34. Lima, M. J., Tavares, P. B., Silva, A. M. T., Silva, C. G., Faria, J. L. Selective photocatalytic oxidation of benzyl alcohol to benzaldehyde by using metal-loaded g-C_3N_4 photocatalysts. *Catalysis Today*. **2017,** *287*, 70-77.

35. Cheng, J., Hu, Z., Li, Q., Li, X., Fang, S., Wu, X., Li, M., Ding, Y., Liu, B., Yang, C., Wen, L., Liu, Y., Lv, K. Fabrication of high photoreactive carbon nitride nanosheets by polymerization of amidinourea for hydrogen production. *Applied Catalysis B: Environmental*. **2019,** *245*, 197-206.

36. Wang, Y., Bai, L., Zhang, Z., Qu, Y., Jing, L. Improved visible-light photoactivity of Pt/g-C_3N_4 nanosheets for solar fuel production via pretreated boric acid modification. *Research on Chemical Intermediates*. **2019,** *45*, 249-259.

37. Da Silva, E. S., Moura, N. M. M., Coutinho, A., Dražić, G., Teixeira, B. M. S., Sobolev, N. A., Silva, C. G., Neves, M. G. P. M. S., Prieto, M., Faria, J. L. Β-Cyclodextrin as a precursor to holey C-doped g-C_3N_4 nanosheets for photocatalytic hydrogen generation. *ChemSusChem*. **2018,** *11*, 2681-2694.

38. Liu, B., Ye, L., Wang, R., Yang, J., Zhang, Y., Guan, R., Tian, L., Chen, X. Phosphorus-doped graphitic carbon nitride nanotubes with amino-rich surface for efficient CO_2 capture, enhanced photocatalytic activity, and product selectivity. *ACS Applied Materials & Interfaces*. **2018,** *10*, 4001-4009.

39. Yang, H., Zhou, Y., Wang, Y., Hu, S., Wang, B., Liao, Q., Li, H., Bao, J., Ge, G., Jia, S. Three-dimensional flower-like phosphorus-doped g-C_3N_4 with a high surface area for visible-light photocatalytic hydrogen evolution. *Journal of Materials Chemistry A*. **2018,** *6*, 16485-16494.

40. Soldano, C., Mahmood, A., Dujardin, E. Production, properties and potential of graphene. *Carbon*. **2010,** *48*, 2127-2150.

41. Dreyer, D. R., Park, S., Bielawski, C. W., Ruoff, R. S. The chemistry of graphene oxide. *Chemical Society Reviews*. **2010,** *39*, 228-240.

42. Hummers, W. S., Offeman, R. E. Preparation of graphitic oxide. *Journal of the American Chemical Society*. **1958,** *80*, 1339-1339.

43. Gusain, R., Kumar, P., Sharma, O. P., Jain, S. L., Khatri, O. P. Reduced graphene oxide–CuO nanocomposites for photocatalytic conversion of CO_2 into methanol under visible light irradiation. *Applied Catalysis B: Environmental*. **2016,** *181*, 352-362.

44. Ramakrishna Matte, H. S. S., Gomathi, A., Manna, A. K., Late, D. J., Datta, R., Pati, S. K., Rao, C. N. R. MoS_2 and WS_2 analogues of graphene. *Angew Chem Int Ed*. **2010,** *49*, 4059-4062.

45. Li, Z., Meng, X., Zhang, Z. Recent development on MoS_2-based photocatalysis: A review. *Journal of Photochemistry and Photobiology C: Photochemistry Reviews*. **2018,** *35*, 39-55.

46. Krishnan, U., Kaur, M., Singh, K., Kumar, M., Kumar, A. A synoptic review of MoS_2: Synthesis to applications. *Superlattices and Microstructures*. **2019,** *128*, 274-297.

47. Zhang, R., Wan, W., Li, D., Dong, F., Zhou, Y. Three-dimensional MoS_2/reduced graphene oxide aerogel as a macroscopic visible-light photocatalyst. *Chinese Journal of Catalysis*. **2017,** *38*, 313-320.

48. Min, S., Lu, G. Sites for high efficient photocatalytic hydrogen evolution on a limited-layered MoS_2 cocatalyst confined on graphene sheets—The role of graphene. *The Journal of Physical Chemistry C*. **2012,** *116*, 25415-25424.

49. Jinliang, L., Liu, X., Pan, L., Wei, Q., Chen, T., Sun, Z. MoS_2–reduced graphene oxide composites synthesized via a microwave-assisted method for visible-light photocatalytic degradation of methylene blue. *RSC Advances*. **2014,** *4*, 9647.

50. Morikawa, M., Ogura, Y., Ahmed, N., Kawamura, S., Mikami, G., Okamoto, S., Izumi, Y. Photocatalytic conversion of carbon dioxide into methanol in reverse fuel cells with tungsten oxide and layered double hydroxide photocatalysts for solar fuel generation. *Catalysis Science & Technology*. **2014,** *4*, 1644-1651.

51. Teramura, K., Iguchi, S., Mizuno, Y., Shishido, T., Tanaka, T. Photocatalytic conversion of CO_2 in water over layered double hydroxides. *Angewandte Chemie (International ed. in English)*. **2012,** *51*, 8008-8011.

52. Silva, C. G., Bouizi, Y., Fornés, V., García, H. Layered double hydroxides as highly efficient photocatalysts for visible light oxygen Generation from water. *Journal of the American Chemical Society*. **2009,** *131*, 13833-13839.

53. Othman, M. R., Helwani, Z., Martunus, Fernando, W. J. N. Synthetic hydrotalcites from different routes and their application as catalysts and gas adsorbents: A review. *Applied Organometallic Chemistry*. **2009,** *23*, 335-346.

54. Rives, V., Angeles Ulibarri, M. a. Layered double hydroxides (LDH) intercalated with metal coordination compounds and oxometalates. *Coordination Chemistry Reviews.* **1999,** *181*, 61-120.

55. Li, C., Wei, M., Evans, D. G., Duan, X. Layered double hydroxide-based nanomaterials as highly efficient catalysts and adsorbents. *Small.* **2014,** *10*, 4469-4486.

56. Yang, Z.-z., Wei, J.-j., Zeng, G.-m., Zhang, H.-q., Tan, X.-f., Ma, C., Li, X.-c., Li, Z.-h., Zhang, C. A review on strategies to LDH-based materials to improve adsorption capacity and photoreduction efficiency for CO_2. *Coordination Chemistry Reviews.* **2019,** *386*, 154-182.

57. Seron, A., Delorme, F. Synthesis of layered double hydroxides (LDHs) with varying pH: A valuable contribution to the study of Mg/Al LDH formation mechanism. *Journal of Physics and Chemistry of Solids.* **2008,** *69*, 1088-1090.

58. Nalawade, P., Aware, B., J. Kadam, V., Hirlekar, R. Layered double hydroxides: A review. *Journal of Scientific and Industrial Research.* **2009,** *68*, 267-272.

59. Quiroz-Cardoso, O., Oros-Ruiz, S., Solís-Gómez, A., López, R., Gómez, R. Enhanced photocatalytic hydrogen production by CdS nanofibers modified with graphene oxide and nickel nanoparticles under visible light. *Fuel.* **2019,** *237*, 227-235.

60. Petrols, B. *BP statistic review of world energy*; 2018; p 10.

61. Yang, Y., Wu, J., Xiao, T., Tang, Z., Shen, J., Li, H., Zhou, Y., Zou, Z. Urchin-like hierarchical CoZnAl-LDH/RGO/g-C_3N_4 hybrid as a Z-scheme photocatalyst for efficient and selective CO_2 reduction. *Applied Catalysis B: Environmental.* **2019,** *255*, 117771.

62. Sakakura, T., Choi, J.-C., Yasuda, H. Transformation of carbon dioxide. *Chemical Reviews.* **2007,** *107*, 2365-2387.

63. Nielsen, D. U., Hu, X.-M., Daasbjerg, K., Skrydstrup, T. Chemically and electrochemically catalysed conversion of CO_2 to CO with follow-up utilization to value-added chemicals. *Nature Catalysis.* **2018,** *1*, 244-254.

64. Diab, K. R., El-Maghrabi, H. H., Nada, A. A., Youssef, A. M., Hamdy, A., Roualdes, S., Abd El-Wahab, S. Facile fabrication of $NiTiO_3$/graphene nanocomposites for photocatalytic hydrogen generation. *Journal of Photochemistry and Photobiology A: Chemistry.* **2018,** *365*, 86-93.

65. Wang, Y., Zhang, Y., Zhao, S., Huang, Z., Chen, W., Zhou, Y., Lv, X., Yuan, S. Bio-template synthesis of Mo-doped polymer carbon nitride for photocatalytic hydrogen evolution. *Applied Catalysis B: Environmental.* **2019,** *248*, 44-53.

66. Rivero, M. J., Iglesias, O., Ribao, P., Ortiz, I. Kinetic performance of TiO_2/Pt/reduced graphene oxide composites in the photocatalytic hydrogen production. *International Journal of Hydrogen Energy.* **2019,** *44*, 101-109.

67. Zhao, H., Sun, S., Wu, Y., Jiang, P., Dong, Y., Xu, Z. Ternary graphitic carbon nitride/red phosphorus/molybdenum disulfide heterostructure: An efficient and low cost photocatalyst for visible-light-driven H_2 evolution from water. *Carbon.* **2017,** *119*, 56-61.

68. Zhang, L., Jin, Z., Huang, S., Huang, X., Xu, B., Hu, L., Cui, H., Ruan, S., Zeng, Y.-J. Bio-inspired carbon doped graphitic carbon nitride with booming photocatalytic hydrogen evolution. *Applied Catalysis B: Environmental.* **2019,** *246*, 61-71.

69. Li, L., Wu, J., Liu, B., Liu, X., Li, C., Gong, Y., Huang, Y., Pan, L. NiS sheets modified CdS/reduced graphene oxide composite for efficient visible light photocatalytic hydrogen evolution. *Catalysis Today.* **2018,** *315*, 110-116.

70. Hernández-Majalca, B. C., Meléndez-Zaragoza, M. J., Salinas-Gutiérrez, J. M., López-Ortiz, A., Collins-Martínez, V. Visible-light photo-assisted synthesis of GO-TiO_2 composites for the photocatalytic hydrogen production. *International Journal of Hydrogen Energy.* **2019,** *44*, 12381-12389.

71. Gil, J. J., Aguilar-Martínez, O., Piña-Pérez, Y., Pérez-Hernández, R., Santolalla-Vargas, C. E., Gómez, R., Tzompantzi, F. Efficient ZnS–ZnO/ZnAl-LDH composite for H_2 production by photocatalysis. *Renewable Energy.* **2019**, *145*, 124-132.

72. Luo, B., Song, R., Jing, D. ZnCr LDH nanosheets modified graphitic carbon nitride for enhanced photocatalytic hydrogen production. *International Journal of Hydrogen Energy*. **2017,** *42*, 23427-23436.

73. Dutch Institute for Fundamental Energy Research. Solar fuels cyclus. https://www.differ.nl/dossier/zonnebrandstoffen-ntvn-special (accessed 25-06-2019).

74. Zhang, F., Zhang, H., Liu, Z. Recent advances on electrochemical reduction of CO_2. *Current Opinion in Green and Sustainable Chemistry*. **2019,** *16*, 77-84.

75. Tang, J.-y., Guo, R.-t., Pan, W.-g., Zhou, W.-g., Huang, C.-y. Visible light activated photocatalytic behaviour of Eu (III) modified g-C_3N_4 for CO_2 reduction and H_2 evolution. *Applied Surface Science*. **2019,** *467-468*, 206-212.

76. Qin, H., Guo, R. T., Liu, X. Y., Pan, W. G., Wang, Z. Y., Shi, X., Tang, J. Y., Huang, C. Y. Z-Scheme MoS_2/g-C_3N_4 heterojunction for efficient visible light photocatalytic CO_2 reduction. *Dalton Transactions*. **2018,** *47*, 15155-15163.

77. Pastrana-Martínez, L. M., Silva, A. M. T., Fonseca, N. N. C., Vaz, J. R., Figueiredo, J. L., Faria, J. L. Photocatalytic reduction of CO_2 with water into methanol and ethanol using graphene derivative–TiO_2 composites: Effect of pH and copper(I) oxide. *Topics in Catalysis*. **2016,** *59*, 1279-1291.

78. Shehzad, N., Tahir, M., Johari, K., Murugesan, T., Hussain, M. Improved interfacial bonding of graphene-TiO_2 with enhanced photocatalytic reduction of CO_2 into solar fuel. *Journal of Environmental Chemical Engineering*. **2018,** *6*, 6947-6957.

79. Iguchi, S., Teramura, K., Hosokawa, S., Tanaka, T. Photocatalytic conversion of CO_2 in an aqueous solution using various kinds of layered double hydroxides. *Catalysis Today*. **2015,** *251*, 140-144.

80. Thommes, M., Kaneko, K., Neimark Alexander, V., Olivier James, P., Rodriguez-Reinoso, F., Rouquerol, J., Sing Kenneth, S. W. Physisorption of gases, with special reference to the evaluation of surface area and pore size distribution (IUPAC Technical Report). *Pure and Applied Chemistry*. **2015,** *87*, 1051.

81. Niemantsverdriet, J. W., Spectroscopy in Catalysis - An introduction. 2nd ed.; GmbH, W. V. V., Ed. 13 July 2000; pp 138-145; 169-179.

82. Ma, Y., Liu, E., Hu, X., Tang, C., Wan, J., Li, J., Fan, J. A simple process to prepare few-layer g-C_3N_4 nanosheets with enhanced photocatalytic activities. *Applied Surface Science*. **2015,** *358*, 246-251.

83. Reddy, K. R., Reddy, C. H. V., Nadagouda, M. N., Shetti, N. P., Jaesool, S., Aminabhavi, T. M. Polymeric graphitic carbon nitride (g-C_3N_4)-based semiconducting nanostructured materials: Synthesis methods, properties and photocatalytic applications. *Journal of Environmental Management*. **2019,** *238*, 25-40.

84. Zhang, Q., Yu, K., Zhao, B., Wang, Y., Song, C., Li, S., Yin, H., Zhang, Z., Zhu, Z. Synthesis of a MoS2@MWNT nanostructure with enhanced field emission and electrochemical properties. *RSC Advances*. **2013,** *3*, 10994-11000.

85. Ma, X., Lv, Y., Xu, J., Liu, Y., Zhang, R., Zhu, Y. A strategy of enhancing the photoactivity of g-C_3N_4 via doping of nonmetal elements: A first-principles study. *The Journal of Physical Chemistry C*. **2012,** *116*, 23485-23493.

86. Fang, H.-B., Zhang, X.-H., Wu, J., Li, N., Zheng, Y.-Z., Tao, X. Fragmented phosphorus-doped graphitic carbon nitride nanoflakes with broad sub-bandgap absorption for highly efficient visible-light photocatalytic hydrogen evolution. *Applied Catalysis B: Environmental*. **2018,** *225*, 397-405.

Appendix A - Chemicals

Molybdenum (VI) oxide (MoO_3 > 99.5%), dicyandiamide ($C_2H_4N_4$ > 99%), ethylenediaminetetraacetic acid (EDTA ≥ 98%), choroplatinic acid hydrate ($H_2PtCl_6 \cdot H_2O$ > 99.995%), ruthenium (II) chloride hydrate ($RuCl_3 \cdot H2O$ > 99.9%) and gold (III) chloride trihydrate ($HAuCl_4 \cdot 3H_2O$ > 99.9%) were purchased from Sigma-Aldrich.

Potassium thiocyanate (KSCN> 98 %) was purchased from Merck KGaA.

(2-Aminoethyl)phosphonic acid ($C_2H_8NO_3P$ >99 %) was purchased from Acros Organics.

Dihydrogen hexachloroplatinate (IV) hexahydrate ($H_2PtCl_6 \cdot 6H_2O$ > 99.9%) and palladium (II) chloride ($PdCl_2$ > 99.9%) were purchased from Alfa Aesar.

Ultrapure water obtained from a Millipore Milli-Q system water purification system (≥ 18 MΩ cm^{-1}) was employed throughout the work.

Appendix B – Instrumentation

The diffuse-reflectance UV-Vis spectra was performed using a JASCO V-560 UV-Vis spectrophotometer, with a double monochromator and a double beam optical system with barium sulfate being the reference. The absorption in the spectra was converted to Kubelka-Munk units by the software of the equipment.

Adsportion of N_2 at 77 K were performed in a Quantachrome Nova 4200e. The surface area (S_{BET}) of the material was calculated by the software of the equipment, applying the Brauner-Emmet-Teller equation.

Photoluminescence measurements were carried out in a JASCO (FP-82000) spectrofluorimeter with a 150W Xenon lamp as light source in emission mode (λ_{exc} =370 nm) using bandwidths of 2.5 nm for emission and excitation.

XRD analysis was performed in a PANalytical X'Pert MPD instrument equipped with a X'Celerator detector and secondary monochromator (Cu Ka k = 0.154 nm, 50 kV, 40 mA; data recorded at a 0.017° step size, 100 s/step).

Scanning electron microscopy was performed in a FEI Quanta 400FEG ESEM/EDAX Genesis X4M instrument.

Transmission electron microscopy was performed using a LEO 906E instrument operating at 120 kV, equipped with a 4 M pixel 28 × 28 mm CCD camera from TRS.

Infra-Red spectra of solid samples was recorded on JASCO V-680 FTIR spectrometer equipped with a DLATGS detector and a MIRacle™ Single Reflection ATR (Attenuated Total Reflection ZnSe crystal plate), PIKE Technologies.

Gas chromatography was performed in an INFICON 3000 Micro GC Gas Analyzer (Agilent) equipped with a Molecular Sieve 5A (MolSieve) column and a micro-thermal conductivity detector (TCD) detector, to quantify the amount of H_2 produced.

Additionally, gas chromatography for product analysis in CO_2 photo reduction was performed in an Agilent 7890A, with 2 detectors (FID and TCD) and 3 dedicated colllums: a ParaPlot Q, a MolSieve and a CP-Wax 52 CB.